LEVEL

NAVAL POSTGRADUATE SCHOOL
Monterey, California

THESIS

A STUDY OF THE UNIPOLAR ARCING
DAMAGE MECHANISM ON SELECTED
CONDUCTORS AND SEMICONDUCTORS

by

Franklin Terrence Ryan

and

Stephen Tucker Shedd

June 1981

Thesis Advisors: F Schwirzke
                     K. E Woehler

SECURITY CLASSIFICATION OF THIS PAGE (When Data Entered)

REPORT DOCUMENTATION PAGE		READ INSTRUCTIONS BEFORE COMPLETING FORM
1. REPORT NUMBER	2. GOVT ACCESSION NO. $AD-A105$	3. RECIPIENT'S CATALOG NUMBER $M94$
4. TITLE (and Subtitle) A Study of the Unipolar Arcing Damage Mechanism on Selected Conductors and Semiconductors		5. TYPE OF REPORT & PERIOD COVERED Master's Thesis; June 1981
		6. PERFORMING ORG. REPORT NUMBER
7. AUTHOR(s) Franklin Terrence Ryan Stephen Tucker Shedd		8. CONTRACT OR GRANT NUMBER(s)
9. PERFORMING ORGANIZATION NAME AND ADDRESS Naval Postgraduate School Monterey, California 93940		10. PROGRAM ELEMENT, PROJECT, TASK AREA & WORK UNIT NUMBERS
11. CONTROLLING OFFICE NAME AND ADDRESS Naval Postgraduate School Monterey, California 93940		12. REPORT DATE June 1981
		13. NUMBER OF PAGES 124
14. MONITORING AGENCY NAME & ADDRESS(if different from Controlling Office) Naval Postgraduate School Monterey, California 93940		15. SECURITY CLASS. (of this report) Unclassified
		15a. DECLASSIFICATION/DOWNGRADING SCHEDULE

16. DISTRIBUTION STATEMENT (of this Report)

Approved for public release; distribution unlimited.

17. DISTRIBUTION STATEMENT (of the abstract entered in Block 20, if different from Report)

18. SUPPLEMENTARY NOTES

19. KEY WORDS (Continue on reverse side if necessary and identify by block number)

Unipolar Arcs
Retrograde Motion
Unipolar Arcing on Grain Boundaries

Plasma-surface Interaction
Microwhiskers
Metallic Glasses

20. ABSTRACT (Continue on reverse side if necessary and identify by block number)

A broad investigation, experimental and theoretical, of the mechanism of unipolar arcing has been conducted. A theoretical discussion of existing unipolar arc models is presented. Experimental and theoretical evidence is used to support the Schwirzke-Taylor Model at the expense of other models. Three current models of arc motion are examined and refuted.

DD $\frac{\text{FORM}}{1 \text{ JAN } 73}$ 1473 EDITION OF 1 NOV 65 IS OBSOLETE
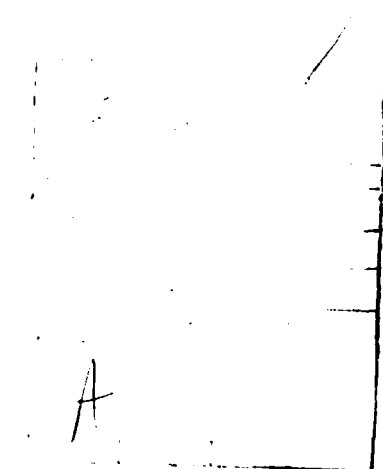(Page 1) S/N 0102-014-6601 |

1 SECURITY CLASSIFICATION OF THIS PAGE (When Data Entered)

#20 - ABSTRACT - (CONTINUED)

Experimental results show that Aluminum and various steels arc heavily, Molybdenum and Nickel to a lesser extent, and commercially prepared metallic glasses not at all. The semi-conductors showed some arcing on Germanium but none on Silicon.

Experiments showed that grain boundaries play no significant role in unipolar arc initiation.

Experiments were conducted in which a laser produced metallic glass is exposed to the plasma produced by the same laser pulse. The results are used to refute the microwhisker explosion models of unipolar arc initiation.

A Study of the Unipolar Arcing
Damage Mechanism on Selected
Conductors and Semiconductors

by

Franklin Terrence Ryan
Lieutenant Commander, United States Navy
B. S., University of Washington, 1969

and

Stephen Tucker Shedd
Commander, United States Navy
B. S., Georgia Institute of Technology, 1968

Submitted in partial fulfillment of the
requirements for the degree of

Master of Science in Physics

from the

NAVAL POSTGRADUATE SCHOOL
June 1981

Author: _____

Author: _____

Approved by: _____
                                        Thesis Advisor

_____
                                        Second Reader

_____
Chairman, Department of Physics and Chemistry

_____
                    Dean of Science and Engineering

3

ABSTRACT

A broad investigation, experimental and theoretical, of the mechanism of unipolar arcing has been conducted. A theoretical discussion of existing unipolar arc models is presented. Experimental and theoretical evidence is used to support the Schwirzke-Taylor Model at the expense of other models. Three current models of arc motion are examined and refuted.

Experimental results show that Aluminum and various steels arc heavily, Molybdenum and Nickel to a lesser extent, and commercially prepared metallic glasses not at all. The semiconductors showed some arcing on Germanium but none on Silicon.

Experiments showed that grain boundaries play no significant role in unipolar arc initiation.

Experiments were conducted in which a laser produced metallic glass is exposed to the plasma produced by the same laser pulse. The results are used to refute the microwhisker explosion models of unipolar arc initiation.

4

TABLE OF CONTENTS

ACKNOWLEDGMENTS

We wish to thank Robert Sanders for his valuable assistance in supporting our work in the plasma laboratory and in obtaining the materials necessary for our experiments. We would like to extend our sincere gratitude to Professor Schwirzke for his advice and guidance throughout this thesis. His suggestions and academic assistance during the experimental work and the writing of this thesis were of great benefit.

I. INTRODUCTION

The interaction of hot plasmas with material surfaces has been investigated since the study of magnetically-confined fusion plasmas began seriously in the early 1950's. Recently, however, the study of plasma-surface interactions has also been directed towards newly emerging technologies such as high energy laser weapons and pulsed power technology which requires the use of high speed plasma switches. Plasma-surface interactions have led to many difficulties in the fusion field. There are, however, two major areas of concern resulting from these interactions. One is that the first wall of the reactor will be damaged by the plasma and by the reaction products. The second is that the particles released by the surface interactions will contaminate the plasma resulting in radiation losses from high atomic number (Z) particles, which in turn, causes sufficient cooling that the plasma cannot be sustained at fusion temperature [1, 2].

There are several different erosion processes which lead to the introduction of impurities into the Tokamak plasma. These different erosion processes are [3]:

1. Sputtering by D, T, He impurity ions and neutrons.

2. Arcing between the plasma and the solid wall (unipolar arcs.)

3. Heat pulses to the first wall which may cause localized evaporation and surface cracking.

8

4. The gas implanted in the first wall can lead to chemical erosion or embrittlement and may cause blistering.

If fusion energy is to become a reality, the problems of containing the plasma long enough at a high enough temperature will depend on controlling these erosion processes due to plasma-surface interaction at the first wall and thus minimizing the release of impurities into the plasma.

Recently, arc tracks have been observed on many surfaces in DITE and have also been found in PLT, ISX, Macrotor, and Pulsator Tokamaks [4, 5]. These arcs occur on the fixed limiter, on probes inserted in the plasma, and on parts of the torus structure. Of most importance, is the evidence that the amount of material removed by arcing is consistent with the concentration of metal impurities in the plasma [5].

With the increasing evidence that unipolar arcing is a severe damage mechanism in plasma-surface interactions, there has been a subsequent flurry of activity in the last several years in studying the arcing mechanism, what conditions initiate arcing, and, subsequently, steps that may be taken to minimize arc damage. At present, there is no universally accepted quantitative model that describes all aspects of unipolar arcing to everyone's satisfaction, but there are many proposed models that are qualitatively appealing and will be discussed in this thesis.

There have recently evolved new areas of technology that will be dependent on our ability to control plasma-surface interactions. Both high energy laser and particle beam weapons systems designs currently use high speed plasma switches to pulse their systems on a microsecond time scale. Present mechanical switches are too slow to achieve the required switching speeds of these emerging technologies and only plasma switches appear to satisfy the design criteria. The problem is that the switch contacts operate in a plasma environment and must be made resistant to arc damage to extend their component lifetime to an acceptable level.

Another area of interest in plasma-surface interaction studies is in assessing the relative importance of the several damage mechanisms to targets of high energy laser weapons systems. It seems quite possible that the effects of plasma-surface interaction could be equally or more damaging to the target than the direct laser-surface interaction damage mechanism. If this turns out to be the case, then the study of plasma-surface interactions could be a vital step in either optimizing our own high energy laser weapons systems effectiveness or in minimizing the damage to our airplanes and missiles from enemy lasers.

The efforts to develop methods of inhibiting arcing damage have included improved surface preparation, optimization of surface material and configuration, and development of new "hard" and arc resistant surfaces.

10

The study reported by this thesis was an investigation of plasma-surface interactions with an emphasis on unipolar arcing susceptibility and damage on selected metals, metallic glasses, and semiconductors. A major portion of this study involved investigating the degree of involvement of grain boundaries and microwhiskers as sites of unipolar arc initiation. In addition, the current unipolar arc model is expanded in this thesis to include proposed models for unipolar arc crater formation and arc cessation. The samples that were investigated included AISI type 304 and 316 stainless steel, AISI type 1010 iron-carbon steel, spectrally pure (.9999) aluminum, molybdenum, three different metallic glasses, silicon and germanium.

A Q-switched neodymium glass laser was used to generate a hot, dense plasma over the target surface which was then examined using optical and scanning electron microscopy to evaluate the effects of plasma-surface interaction on the different target materials.

II. BACKGROUND AND THEORY OF UNIPOLAR ARCING

A. UNIPOLAR ARCING PROBLEM

The interest in unipolar arcing between a hot plasma and hard surfaces has heightened considerably since a 1978 study by Goodall and McCracken reported physical evidence of arcing in the DITE tokamak [5]. They observed that unipolar arcing does occur on test probes, limiters, and the first wall itself; and that this damage mechanism is the dominant one. Perhaps of more importance is the conclusion of this study that the concentration of high-Z impurities in the plasma is consistent with the amount of material removed by arcing. Since that report, arc tracks have also been found in PLT, ISX, Macrotor and Pulsator Tokamaks [4].

The evidence, to date, is conclusive that unipolar arcing is a primary source of high-Z impurities in the fusion plasma. The contamination of the plasma by these high atomic number, Z, particles results in radiation losses which cause sufficient cooling that the plasma cannot be sustained at fusion temperature [6, 7]. The recognition that the control of unipolar arcing is vital to the progress of power generation fusion programs has led to a renewed emphasis in this area of research. The current studies aimed at inhibiting arcing damage have concentrated on controlling arcing through improved

12

surface preparation, optimization of wall and limiter
configuration, and the development of improved materials.

B.   PREVIOUS UNIPOLAR ARC STUDIES

   1.   Robson and Thonemann (1958)

        The first model of unipolar arcing was that proposed
by Robson and Thonemann in 1958 [4]. Although over twenty
years old, this model is still quoted in almost every
current study of unipolar arcing, primarily because it
seems to accurately describe the basic unipolar arc process.
This model, however, leaves a lot to be desired in that it
does not present a very detailed description of the arc and
fails to describe many of the mechanisms attendant with
unipolar arcing such as arc initiation, cathode formation,
and arc cessation. As a result, the Robson and Thonemann
model is used primarily as a reference to the basic arc
mechanism and as a starting point for more detailed models.

        Robson based his theoretical discussion on the works
of Langmuir and Bohm. From these works it is known that
when a plasma and electrically isolated metal are in equi-
librium, a floating sheath potential (V_f) is established
such that the ion and electron leakage rates from the plasma
to the wall are equal. However, within the plasma the ion
temperature (T_i) does not necessarily equal the electron
temperature (T_e). Due to their small mass compared to the
ions, the electrons have a much higher thermal velocity

13

and will initially have a higher leakage rate from the plasma to the wall. As a result, the wall will reach a negative potential relative to the plasma separated by a sheath of width on the order of the Debye length (λ_D). This potential sheath serves to confine electro-statically the more mobile electrons [8]. The plasma potential will build up to the level where ion losses match electron losses, thus maintaining plasma neutrality (Figure 1).
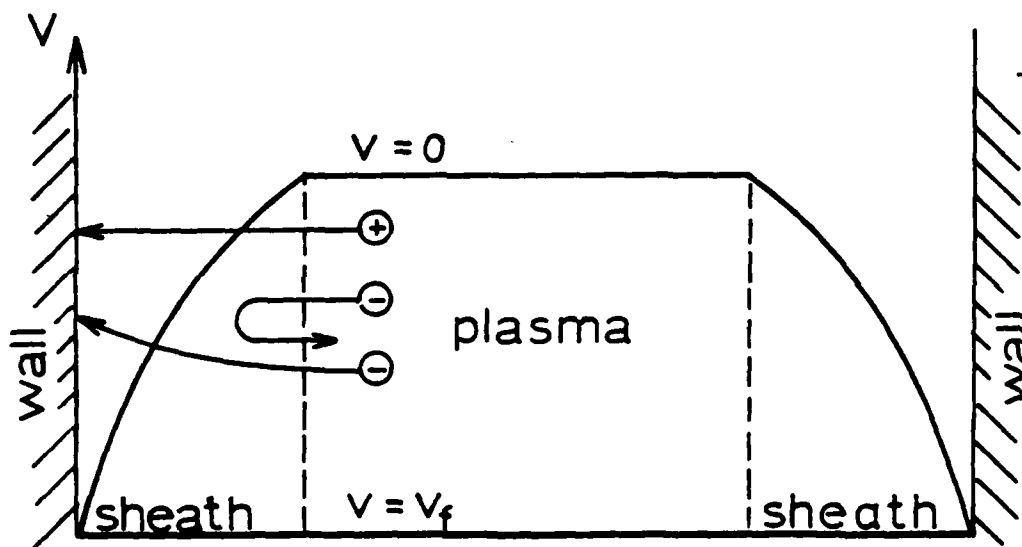

Figure 1.

The confining electric field, E, in the sheath is of the order [7]

$$ E = \frac{-V_f}{\lambda_D} $$

where: V_f = floating or sheath potential

14

$$\lambda_D = \text{Debye Length} = \left(\frac{kT_e}{4\pi ne^2}\right)^{\frac{1}{2}}$$

n = Plasma density

T_e = electron temperature

k = Boltzman constant

e = Electron charge

Only electrons in the high energy tail of the Maxwellian velocity distribution can overcome the sheath potential and reach the wall, while the others are turned back to the plasma. On the other hand, ions entering the sheath are all accelerated in the sheath potential and gain energy. Therefore, the sheath potential of the plasma is a self-regulating phenomena that adjusts itself to maintain an even flow of ions and electrons to the wall. The sheath potential is equal to [9]

$$V_f = \frac{kt_e}{2e} \ln \left(\frac{M_i}{2\pi Me}\right)$$

Where: M_i = ion mass

M_e = electron mass

In the Robson model, the diagram of the plasma in the vicinity of the wall can be represented graphically as in Figure 2.

If the electron temperature (T_e) is sufficiently high, V_f will exceed the potential difference required to sustain an arc [9] . If, under these circumstances, a cathode spot is initiated on the plate, the strong local emission of electrons will reduce the sheath potential from V_f to V_c, where V_c is the cathode fall potential of the arc. More electrons can now reach the plate against the retarding potential. A circulating current is thus set up, electrons being locally emitted from the cathode spot and returning uniformly over the rest of the plate, satisfying the condition that the total current to the plate shall be zero. Therefore, there are two possible equilibrium conditions. In the first case, the plate is at V_f ($V_f < 0$) with respect to the plasma and there is no arcing. In the second case, the plate is at V_c ($|V_c| < |V_f|$) and there is a circulating current (I_c) through a cathode spot (Figure 3).

The circulating arc current is given by [9]

$$I_c = Ane \left(\frac{kT_e}{2 \pi m_e} \right)^{\frac{1}{2}} \left(\exp \left\{ \frac{-eV_c}{kT_e} \right\} - \exp \left\{ \frac{-eV_f}{kT_e} \right\} \right)$$

Where:

      A = area of plate

      V_c = cathode fall potential

In his model, Robson contends that there is a minimum current (I_a) necessary to maintain a stable cathode spot and that as long as I_c is greater than I_a, the cathode spot, once initiated, is maintained. Robson's model indicates that I_c is directly proportional to the area of the plate and the plasma density, indicating that below a critical plate size or a plasma density, unipolar arcing will not be sustained.

As mentioned earlier, this model is very general and leaves many areas of unipolar arcing unexplained. For instance, when will V_f exceed the potential required to sustain an arc, what initiates a cathode spot on the plate, what minimum current (I_a) is necessary to maintain a stable cathode spot, and why the cathodes fall potential (V_c) can be assumed uniform over the plate--all remain unanswered in this model. Basic numbers used in conjunction with this model have orders of magnitude as follows [1] :
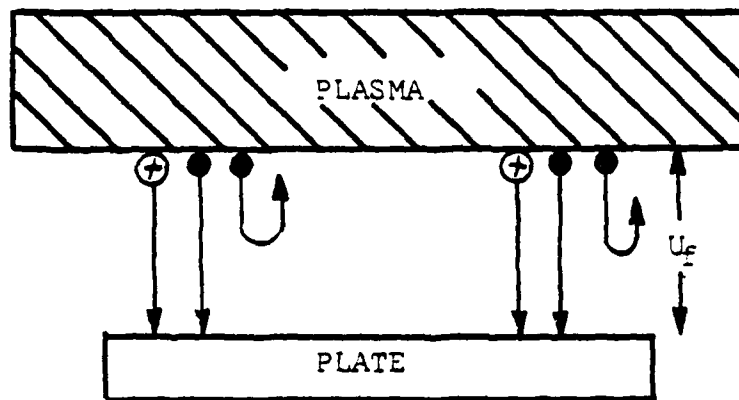
$$V_f = 10 \text{ volts} \qquad I_a = 10 \text{ Amperes}$$

$$kT_e = 2.0 - 3.5 \text{ ev} \qquad A_{min} = 1 \text{ cm}^2$$
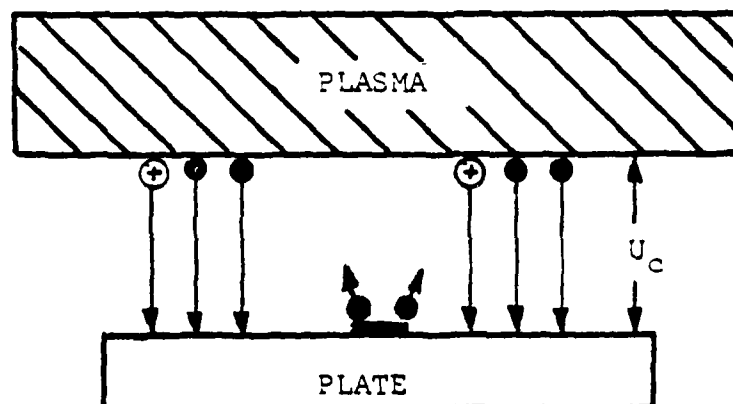
2. **George H. Miley** (1976)

George H. Miley proposed an expanded version of the Robson Model which predicted erosion rates in Tokamaks due to unipolar arcs of approximately two orders of magnitude

17

⊕ ION   ● ELECTRON

Figure 2.   Equilibrium of isolated plate with no cathode spot.

⊕ ION   ● ELECTRON

Figure 3.   Equilibrium of isolated plate with a cathode spot.

18

greater than for normal ion sputtering [10] . These numbers
have been shown to be fairly accurate in later studies of
arcing in DITE Tokamak by Goodall and McCracken [5] . In
this model, Miley proposes that unipolar arcing occurs when,
due to surface imperfections, small hot spots occur on the
wall. The temperature at these cathode spots can be suffi-
cient to cause rapid evaporation of the local wall material,
resulting in serious erosion problems. The proposed mecha-
nism in this model that allows the formation of these hot
spots is that small inclusions or insulating areas in the
surface charge up and eventually explode into an arc [1] .

C. CURRENT UNIPOLAR ARC MODEL

The most recent unipolar arc model in the literature
was proposed by F. Schwirzke and R. Taylor in 1978. This
model starts with the same conditions existing between a
hot plasma and a surface as in previous models. The condi-
tion of plasma quasi-neutrality leads to the formation of
a potential sheath of width approximately equal to the
Debye length (λ_D). The plasma assumes a positive sheath
or floating potential with respect to the wall of [9]

$$V_f = (kT_e/2e) \ln \left(\frac{M_i}{2 \pi m_e} \right)$$

The sheath width is given by [8]

$$\lambda_D = (kT_e/4 \pi n_e e^2)^{\frac{1}{2}}$$

19

and the electric field in the sheath is considered to be
approximately [7]

$$E_{sheath} = V_f / \lambda_D = \pi^{\frac{1}{2}} \ln (M_i / 2\pi m_e) (n_e)^{\frac{1}{2}} (kT_e)^{\frac{1}{2}}$$

where:

M_i = mass of ions

m_e = electron mass

n_e = electron density

Unipolar arcing occurs if the field strength in the
sheath increases enough to ignite and sustain an arc. Elec-
trons are then emitted from a cathode surface spot into the
plasma by temperature-aided field emission. [11, 12] . In
this model for an arc to develop it is necessary that the
ion density increases in front of the cathode spot in order
that a larger electron current can flow into the plasma.
The ion density can increase by ionization of neutral atoms
which are released locally from a "hot" surface spot.
Surface protrusions, metallurgical inhomogeneities, and
inclusions can produce a localized enhancement of the field
strength by a factor of up to 100 [13] . This increased
electric field strength will increase the ion flux from the
plasma to these spots (Figure 4). The increased ion
bombardment and recombination rates lead to locally in-
creased surface temperature at the cathode spot. This local

heating leads to desorption of gases, vaporization of oil films, and the evaporization of neutral metal atoms into the sheath and plasma. The localized surface heating is enhanced by the lower thermal conduction rate from projections and dielectric inclusions compared to the surrounding metal surface. The probability for ionization of a neutral atom in or near the sheath is of the order (Debye length)/ (electron mean free path length) <<1 [7]. Therefore, a small fraction of these released neutral atoms will be ionized in the sheath by electrons in the high energy tail of the Maxwellian distribution, resulting in a local increase in density of the plasma above the cathode spot. The vast majority of the released neutrals would then be ionized in the plasma. This small fraction of neutrals ionized in the sheath, however, could be expected to triple the existing local plasma density [7]. Since the sheath width is inversely proportional to the square root of the plasma density and the electric field strength is directly proportional to the square root of the plasma density, there will be a local narrowing of the sheath width above the cathode spot and an increase in the electric field strength. The ions produced in the sheath would then be accelerated in the sheath potential and fall rapidly back to the cathode spot (Figure 5). This increased ion bombardment acts as a feedback mechanism which leads to further

21

surface heating, metal evaporization, ionization, and increasing plasma density.

The local increase in the plasma density over the cathode spot in addition to decreasing the sheath width and increasing the electric field strength across the sheath, creates a radial pressure gradient, ∇P, over the cathode spot. This pressure (density) gradient forms another electric field, E_R, in the radial direction tangential to the surface of [7]

$$E_R = - \left(\frac{kT_e}{e} \right) \left(\frac{1}{n} \right) \left(\frac{dn}{dr} \right)$$

where: $\frac{dn}{dr}$ = density gradient over cathode spot

This radial electric field is created by the ambipolar diffusion of the more mobile electrons $(T_e > T_i)$ from the higher pressure region which leads to a space charge separation and the establishment of the radial field. The faster migration of the electrons from the higher density region lowers the sheath potential in a ringlike area surrounding the higher plasma pressure region directly over the cathode spot. The ions, however, diffuse much more slowly, resulting in a higher ion concentration and an increased sheath potential, U_f, directly over the cathode spot.

22

The electric field across the sheath which initiates and sustains the arc, E_{arc}, is equal to [7]

$$E_{arc} = \frac{U_f}{\lambda_D}$$

Since there has been a local increase in U_f and a decrease in λ_D, there is a large local increase in the electric field strength between the cathode spot and the plasma. The increased ion bombardment and recombination at the cathode spot leads to local heating which, in turn, reduces the field strength required for electron emission. The arc is initiated when the field strength, E_{arc}, is intense enough for the temperature-aided field emission of electrons from the cathode spot to begin. The arc current loop is completed by the return flow of the larger number of electrons from the high energy tail in the Maxwellian distribution that can now overcome the lowered sheath potential surrounding the cathode spot and reach the surface. Figure 6 is a diagram of this unipolar arc model.

The main difference between this model and those proposed by Robson and Miley, is that it specifies that the arc return current flows in a ring of diameter just greater than the cathode spot rather than uniformly over the entire surface area. This has the further implication that the idea that arcing can be prevented by using insulated areas (A) smaller than a certain critical size is no longer valid [10] .
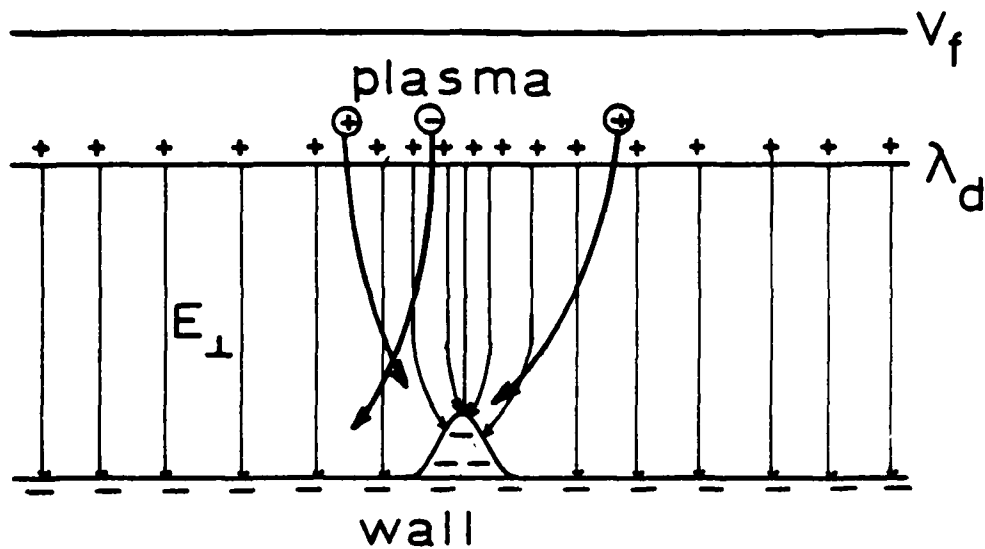
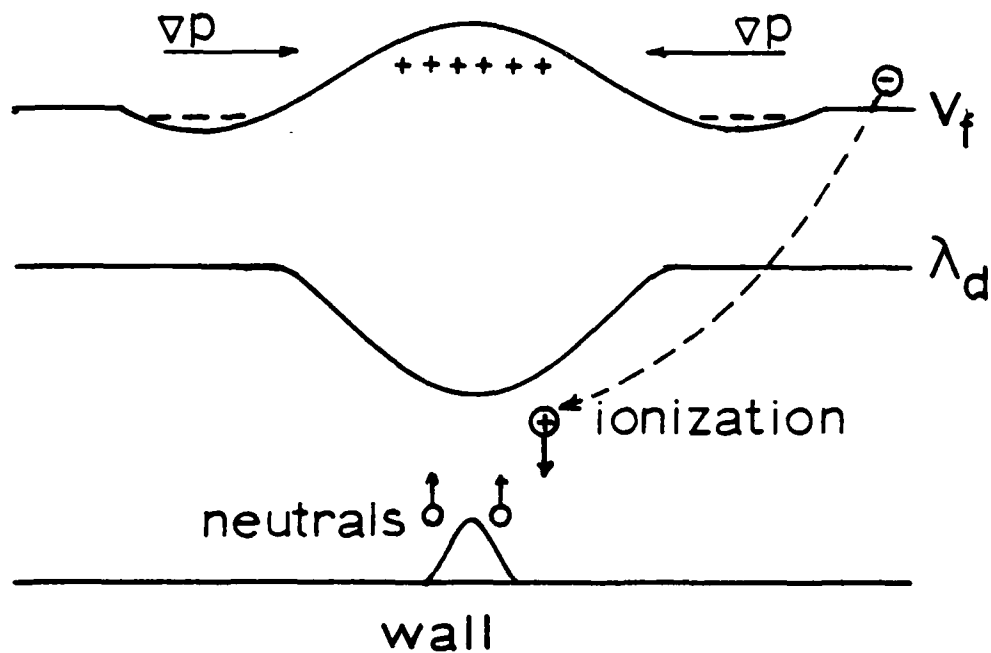Figure 4.   Field Enhancement at Surface Inhomogeneity.

Figure 5.   Increased Plasma Density over cathode spot due to ionization of evaporated neutrals produces narrower sheath width and increased ion bombardment and recombination at the cathode spot.

D. PROPOSED MODEL FOR CRATER FORMATION AND ARC CESSATION.

All of the models described in this thesis conclude with the initiation of the arc and the completion of the return current loop for the electrons. The mechanisms which form the unipolar arc craters and cause arc cessation have been addressed by others [11, 14] , but their models differ widely and do not account for the crater shapes observed in most experiments.

The unipolar arc craters consist of a dark cathode spot about 1-2 μm in diameter and 3-6 μm in depth. The cathode spot is in the center of a hemispherical crater about 10-15 μm in diameter surrounded by an elevated rim that appears to be formed by the material pushed radially from the hemispherical crater. The model proposed in this thesis is consistent with the Schwirzke and Taylor model and the observed crater formations.

1. <u>Crater Formation</u>

This model for crater formation begins with the same conditions existing at arc initiation and current loop establishment as in the model proposed by Schwirzke and Taylor. The sheath width, λ_D, is decreased above the cathode spot, and the sheath potential, U_f, has a local maximum at the cathode spot surrounded by a ring of lowered potential which allows the return flow of electrons which completes the current loop. The arc current is initiated when the field strength at the cathode spot, E_{arc}, is

25

PLASMA

SHEATH

SURFACE

ELECTRONS

IONIZATION

CATHODE SPOT

NEUTRAL ATOM

∇p_e

E_r

E_r

E_{arc}

e^-

e^-
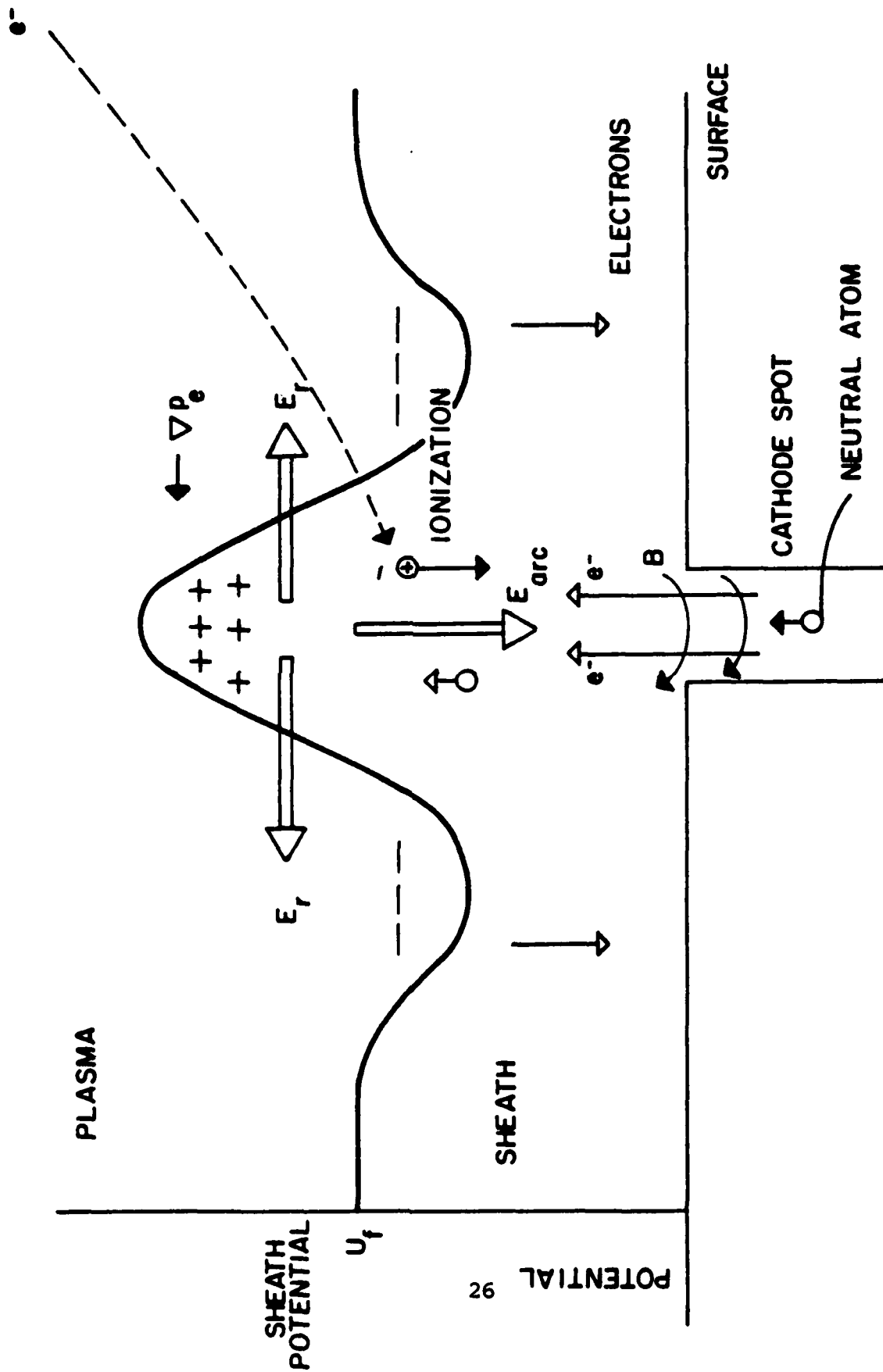
B

SHEATH POTENTIAL

U_f

POTENTIAL

26

Figure 6. Unipolar Arc Model.

sufficient to start the temperature-aided field emission of electrons (Figure 7).

Once the arc is initiated, the joule heating due to the current flow through the cathode spot adds to the localized heating due to ion bombardment and recombination. This additional heating causes accelerated metal evaporation and increased neutral density above the cathode spot. The increased neutral density will allow a larger fraction of neutrals to be ionized, since the electron mean free path length for ionizing a neutral is inversely proportional to neutral density as [7]

$$\lambda_e = 1/(n_o \sigma)$$

where

n_o = neutral density

σ = ionization cross section
of neutral

This provides an increasing local plasma density, an increased ion bombardment at the cathode, and a decreased sheath width. Because of the additional local heating, the electron emission mechanism shifts from field dominated emission to thermionically dominated emission. The arc current, I_a, which is primarily due to electron flow [11] , has an estimated value on the order of 10 Amperes [4, 10] . This current, flowing through a cathode spot of radius $r = 0.5$ μm, creates a pinch magnetic field, B_θ ,

27

of 40,000 G [7] . The pinch magnetic field, B_θ , forces the emitted electrons to exit in a narrow jet while, simultaneously, rejecting electrons that attempt to cross the sheath from the walls of the forming crater. Figure 8 is a diagram of the unipolar arc early in this crater development stage.

As the arc continues, the thermal emission of electrons and neutrals erodes the cathode spot. The emitted neutral vapor jet becomes more directed as the crater becomes deeper. This leads to a more peaked plasma density distribution over the cathode spot which reduces the sheath width, λ_D, to a magnitude much less than the dimensions of the arc crater. This means that the plasma will exist inside the arc crater. For example, for a local plasma density of 10^{18} cm^{-3}, the sheath width, λ_D, is approximately equal to 10^{-6} cm which is much less than the cathode spot diameter of 1 μm [7] . In the initial stages, most of the ionization is created by high energy electrons in the plasma. However, as the crater develops and a high density plasma is formed in the crater, the emitted electrons from the cathode spot which are accelerated in the sheath contribute to the ionization of neutrals. In order for the arc to sustain itself, another condition is imposed on the plasma. This condition is that the sheath potential, U_f, above the cathode spot is equal or larger than the ionization energy, U_i, of the neutral atoms. This allows the

28

emitted electrons to acquire enough energy while crossing the sheath to ionize the emitted neutrals. The ionization energy for Fe is U_i = 7.9 ev. The sheath potential for Fe plasma is [7]

$$U_f = 4.85 \frac{kT_e}{e}$$

where

T_e = electron temperature in plasma

This implies the minimum electron temperature to sustain the arc is kT_e = 2 ev. Since $kT_e \gg$ 2 ev, this condition is easily met. The ionization of neutrals by high energy electrons from the plasma is supplemented by the increased ionization of neutrals over the cathode spot by the accelerated and magnetically confined beams of electrons emitted from the cathode surface at the bottom of the crater. At the resulting high plasma density in the crater, the confinement of electrons now represents a hollow cathode configuration and the ionization rate should be high [7]. For example, a 1 μm diameter by 3 μm deep crater has a volume V = 2.35 x 10^{-12} cm^3. For Fe, this amounts to 2 x 10^{11} neutral atoms being emitted over the arc lifetime. If a 30 nanosecond arc is assumed and the velocity of the emitted neutrals is taken to be equal to the thermal velocity (10^5 cm/sec) associated with the melting temperature (1526 C) of Fe, the neutral density in the crater is
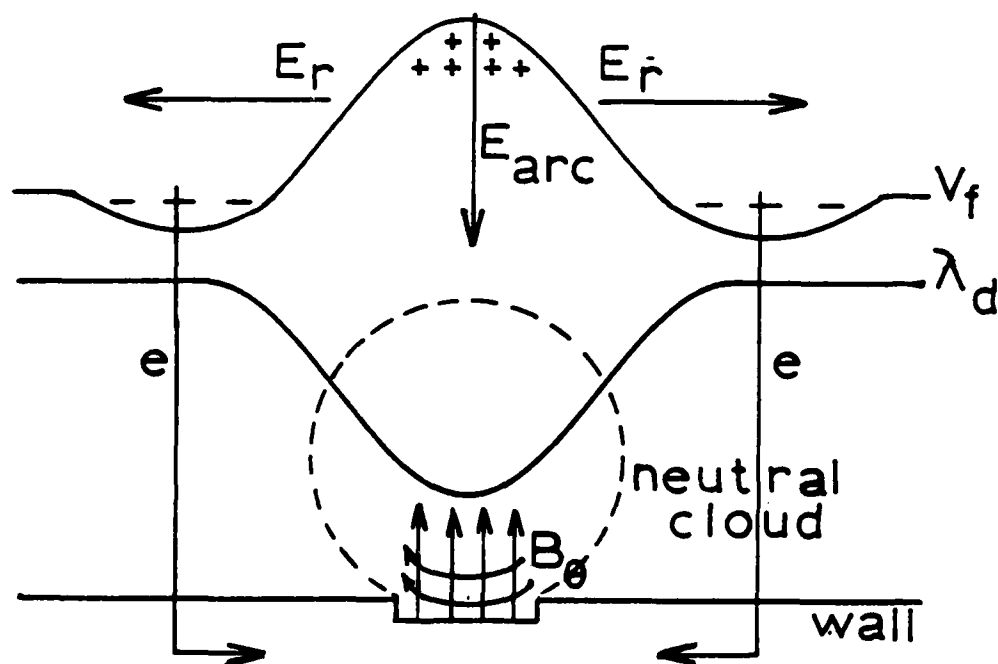
29
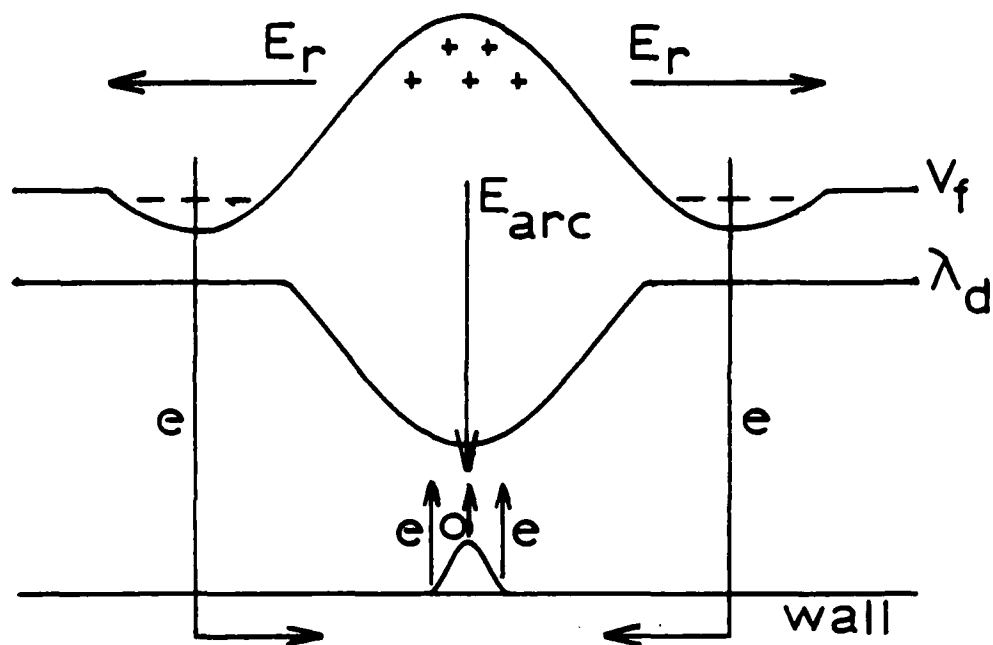
Figure 7. Initiation of Arc.

Figure 8. Early in Crater Development.

approximately equal to 1.5×10^{19} cm^{-3}. The fraction
ionized within 2 μm from the bottom of the crater is on
the order of 2 μm/$\lambda_e \cong 0.03$. This would give a very high
plasma density within the crater of about 10^{18} cm^{-3}. The
hollow cathode configuration would probably allow an even
higher fraction of the neutrals to be ionized inside the
crater, further increasing the plasma density. As the arc
is burning, the area surrounding the arc hole is being
heated by the increased local ion bombardment and recombi-
nation energy given off at the surface immediately surround-
ing the arc spot. In addition, the plasma jet emitted from
the crater expands radially due to the strong pressure
gradient above the arc hole. As the surface surrounding
the arc hole becomes molten, the material is forced out in
a radial direction by the pressure of the expanding plasma,
forming the distinctive rims that have been observed. The
longer the arc burns, the more the plasma expands and the
surface melting will occur over a larger area. This, in
turn, will result in a wider crater rim diameter. Figure 9
is a diagram of the fully developed arc crater.

2. Arc Cessation

As the arc hole grows deeper, a plasma density
profile with a maximum in the crater is established. Figure
10 shows the arc hole and the plasma density profile for
this model. Due to the ionization by the electrons emitted
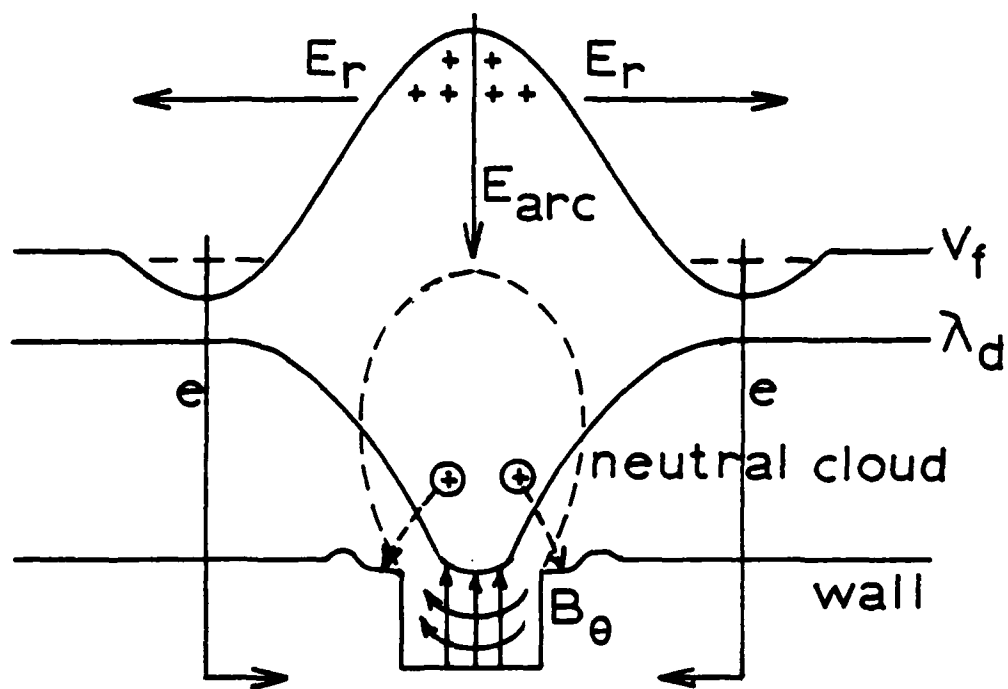from the cathode surface on the bottom of the arc hole, the

31

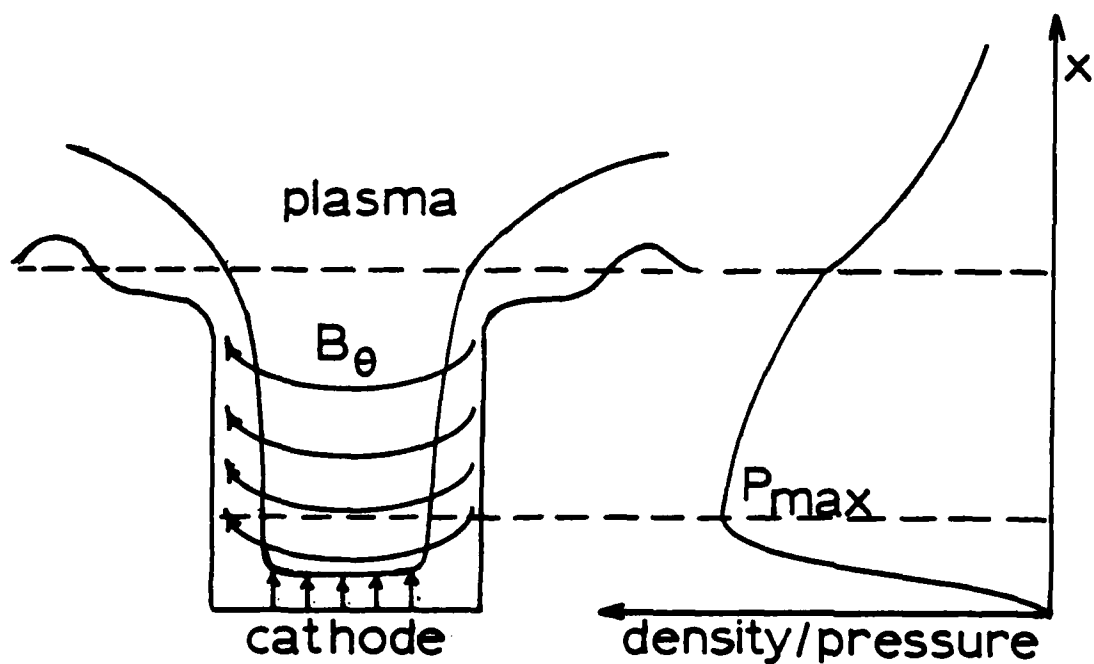Figure 9. Fully Developed Unipolar Arc Crater.

Figure 10. Arc Crater and Corresponding Plasma Density Profile.

density profile assumes a maximum which falls off toward the top of the arc hole. The resulting pressure gradient forces the plasma above P_{max} out of the arc hole in a jet, while below P_{max}, it forces the ions even faster into the sheath where they are further accelerated to the cathode spot.

However, for the arc to be sustained it is necessary that a sufficient sheath potential, U_f, be maintained above the ionization energy of the neutrals. The sheath potential, on the other hand, is ultimately maintained by the thermal energy of the original plasma electrons where

$$U_f = (\text{constant}) \times \frac{kT_e}{e}$$

The energetic main plasma established by the laser heating is the source of energy for establishing the sheath potential and providing the driving emf for the arc current. When the neutral and plasma density in the arc hole increases to a high enough level, the main plasma electrons will be unable to get across the pressure (density) gradient at P_{max} with enough energy (kT_e) to maintain the sheath potential above the cathode spot above the minimum value required to sustain the arc. The energetic main plasma electrons lose energy in the high neutral (and plasma) density region in the arc crater due to increased ionization and excitation rates. This represents

33

a cooling of the plasma in the high density region which lowers the sheath potential even more markedly since it is proportional to the electron temperature times a mass factor dependent on the wall material. For Fe, the sheath potential is

$$U_f = 4.85 \frac{kT_e}{e}$$

This means that for Fe, a 1 ev drop in plasma temperature produces a 5V reduction in the sheath potential U_f. When the sheath potential drops below the potential required to sustain the arc, the arc ceases and the current loop is broken. The plasma cooling in the high density region of the arc crater amounts to a decoupling of the plasmas and the plasma energies.

III. EXPERIMENTAL DESIGN

A. EQUIPMENT

The equipment used in this thesis to evaluate plasma-surface interactions included a neodymium glass laser and an evacuated target test chamber. A scanning electron microscope and an optical microscope were used to study the surface damage on target samples. Figure 11 is a schematic of the laser and the test chamber arrangement.

The neodymium glass laser was used to irradiate the targets mounted in the test chamber. Following exposure to the laser produced plasmas, the targets were then studied using optical and scanning electron microscopes to determine the extent of surface interaction on each sample.

1. Laser System

A KORAD K-1500Q-switched neodymium doped glass laser [15] , which emits a wavelength of 1.06 micrometers, was the energy source used to produce a hot, dense, plasma over the target surfaces. A detailed description of the installation is given by Davis [16] . In figure 12 a block diagram of the basic components of the system is shown.

Laser output energy may be changed by varying the voltages applied to the oscillator and amplifier flashlamps. During the experiment, however, it was found to be more practical and reliable to change the laser energy levels on the target by inserting filters of varying transmittance in
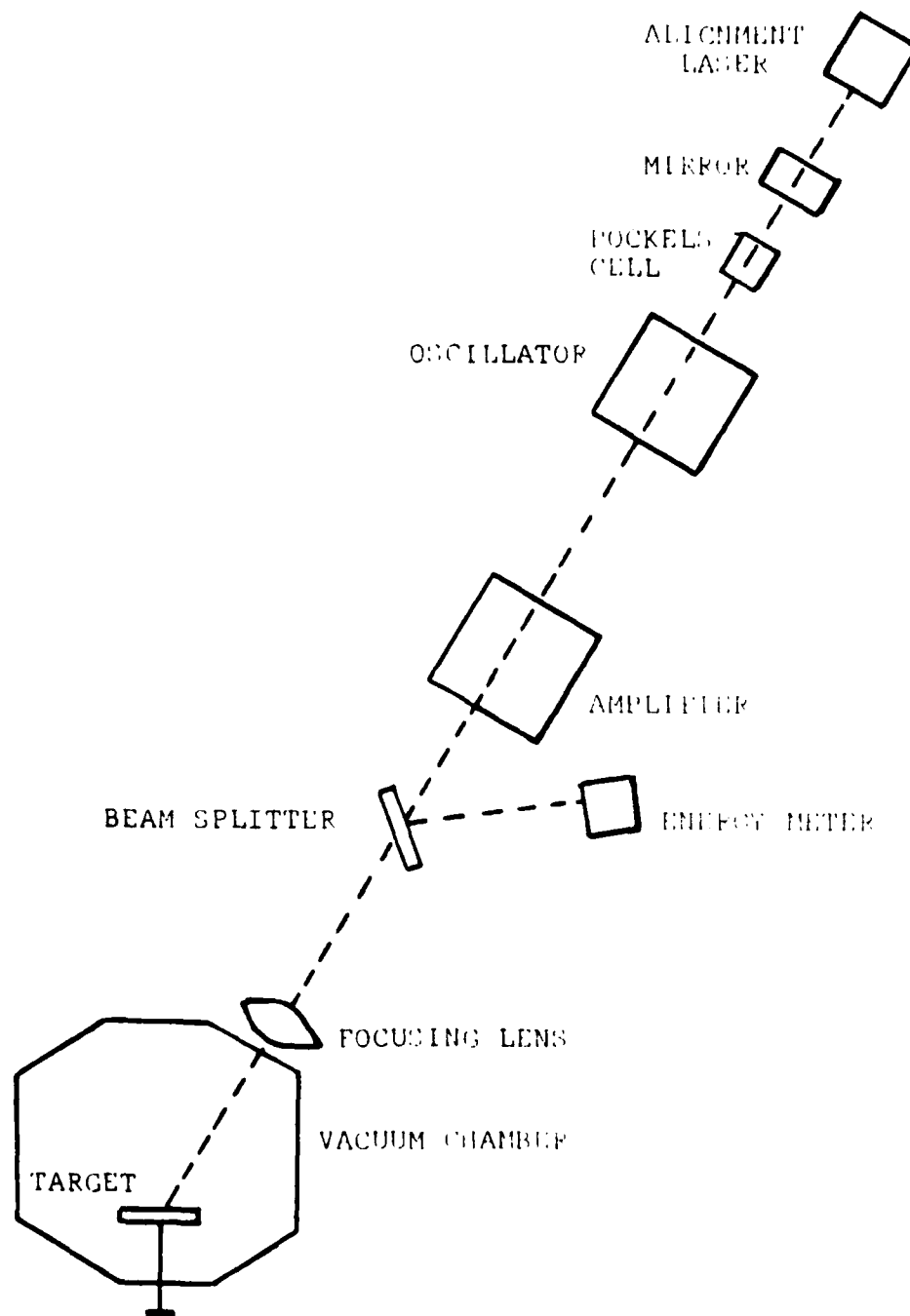
35

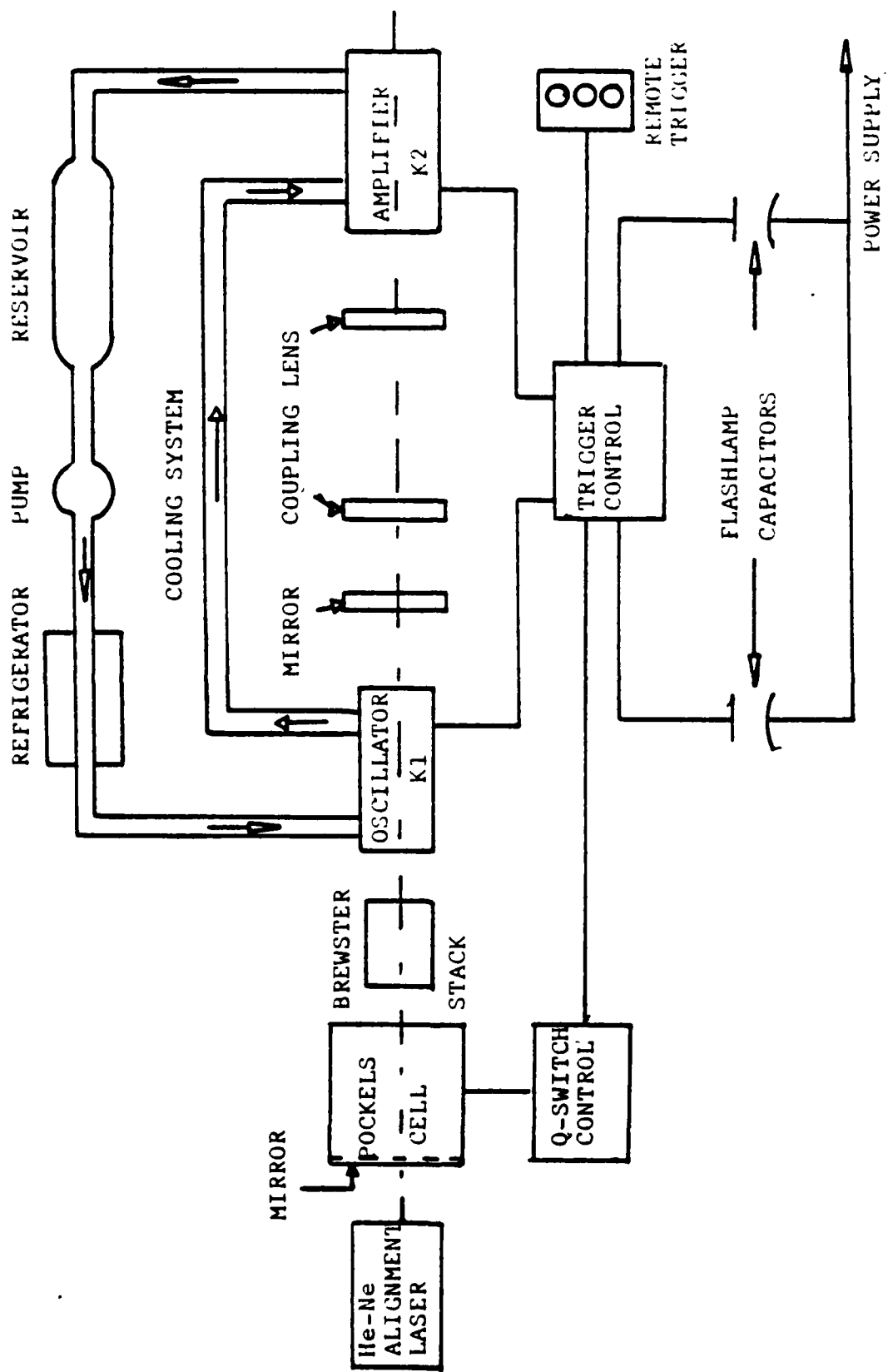Figure 11.   Laser and Test Chamber Arrangement.

Figure 12. The laser system.

the path. The normal output energy range is 0.2-15 J with nominal 25 nanosecond pulse width. These small pulse widths are achieved by a pockels cell Q-switching device mounted between the oscillator and the rear reflector. The unfocused laser beam has a cross-sectional area of 4.04 $\pm$ .2 cm^2 [15] .

For these experiments, the laser was operated at an output level of 7.5 - 12.5 J with the incident energy level on the target varied from 2.1 - 6.4 J using various transmission filters. The laser was focused to an impact area on the target of about 1.13 x 10^{-2} cm^2, giving an irradiance from 185-566 joules/cm^2. The laser total output energy was measured using a Laser Precision RK-3200 Series Pyroelectric Energy Meter.

2. Target Test Chamber

The target test chamber is a 6 inch cube of unbaked aluminum with an internal volume of 12.9 $\pm$ 0.3 liters. The vacuum system was capable of providing a base pressure up to 10^{-6} Torr. The laser beam was aligned 30 degrees from normal to the target surface. A probe was used to hold the targets in the chamber and to rotate the target holder to expose fresh targets without requiring the vacuum in the chamber to be broken. The target holder was designed to hold up to four individual targets. Several ports in the chamber provide for the mounting of gauges as well as observation windows. Figure 13 is a diagram of the target test chamber.
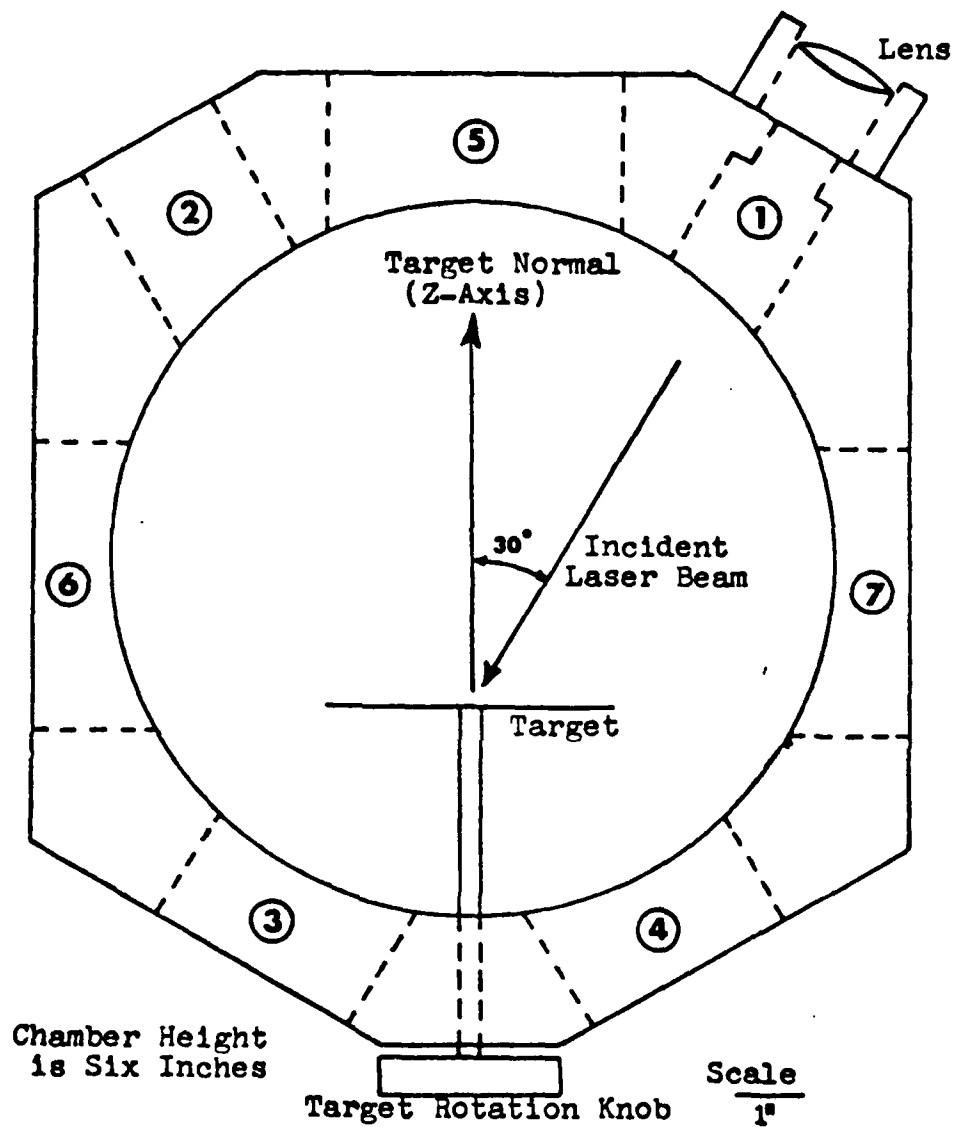
Figure 13.   Top view of vacuum chamber.   Port #1 is the
laser beam entry port, #2 is the reflected
laser beam observation port, #3 is the trans-
mitted laser beam observation port, ports
numbered 4, 5, 6, and 7 are optical/probe
observation ports.   There is also an optical/
probe port in the top of the chamber.

39

3. Optical Microscope

A Zeiss Universal M incident light photomicroscope was used to observe and photograph the target surfaces. The optical magnification with available lenses ranges from 50-650X and the magnification range for photomicroscopy is 65-1000X. This microscope was also used to determine the depths of craters after laser irradiation.

4. Scanning Electron Microscope

The Scanning Electron Microscope used in this work was a Cambridge Stereoscan S4-10. The Stereoscan has a direct reading magnification system which provides a useful range between 20X and 100,000X corresponding to scanned areas of 5 mm to 2 μm square on the specimen. The basic advantage of scanning electron microscopy is that it provides a large depth of field even at the highest levels of magnification which is necessary for complete target surface evaluation. A schematic showing the basic functional assembly of the stereoscan S4-10 is shown in figure 14.

B. PROCEDURES

The experimental procedures can be categorized into three distinct stages: target preparation, plasma-surface interaction, and surface damage evaluation. Target preparation included machining of the samples to fit the target holder, polishing the samples, and examination of
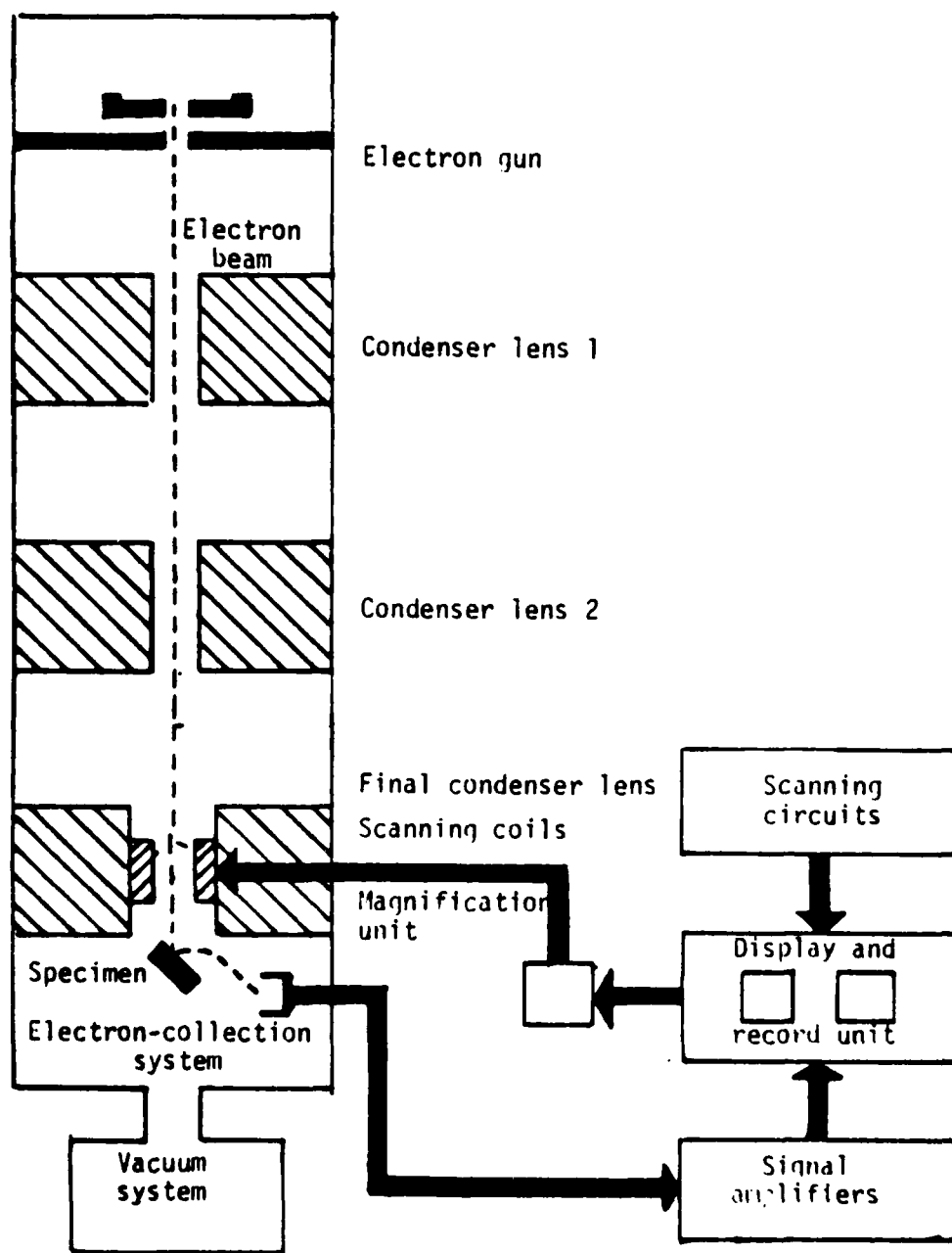
Figure 14.   Scanning electron microscope.

the finished surfaces with optical and scanning electron microscope prior to plasma-surface interaction. The plasma-surface interaction step was accomplished in the plasma laboratory using the neodynium glass laser and the target test chamber. The final step, surface damage evaluation, was accomplished by re-examining each of the samples under both the optical and scanning electron microscope.

1. Target Preparation

The targets made of type 304 or 316 stainless steel, molybdenum, and spectrally pure (.9999) aluminum were machined into discs of 0.5 inch diameter and 0.25 inch thickness to fit the target holder designed for use in the test chamber. The metallic glasses provided by Professor Wagner at UCLA were only available in thin ribbons and had to be mounted onto the machined discs using a highly conductive silver-based adhesive. The remaining samples were the semiconductors, silicon and germanium, which were too brittle for machining and had to be ground to a size adaptable to the target holder.

All targets were then polished using standard metallurgical techniques with a final polishing slurry of 0.05 AL_2O_3 [17] to reduce surface irregularities that tend to promote arcing and to provide an approximately common surface roughness for post plasma-surface interaction comparison of unipolar arcing susceptibility for the different specimens. The polished targets were then examined

42

both under the optical and scanning electron microscope to facilitate comparison with the target surfaces after plasma-surface interaction.

2. Plasma-Surface Interaction

Each target was cleaned with acetone and mounted on the target holder in the test chamber. The laser was focused onto the target and fired at energy levels of 2.1 - 6.4 Joules at a Q-switched pulse duration of 25 nanoseconds. Material from the target surface was vaporized and heated by the incoming laser to form a hot, dense plasma of short duration expanding radially and normal to the target surface. The plasma establishes a sheath potential which leads to unipolar arcing damage.

3. Surface Damage Investigation

Each target surface was examined after laser irradiation using the optical microscope and the scanning electron microscope to determine the nature of plasma-surface interaction and to detect the presence and relative density of unipolar arc craters. The optical microscope was used to determine arc crater depth by focusing on the target surface then refocusing on the bottom of the crater, the difference in focal distance being crater depth.

IV. EXPERIMENTAL RESULTS OF LASER INDUCED
PLASMA-SURFACE INTERACTIONS

This section of the thesis included the evaluation of laser induced plasma-surface interaction on three different categories of target materials: conductors, semiconductors, and metallic glasses. The conductors evaluated included AISI type 304 stainless steel, spectrally pure (.9999) aluminum, molybdenum, and nickel. The semiconductor materials investigated were silicon and germanium. Finally, the last category of materials investigated were three different alloys of metallic glass provided by Professor Wagner at UCLA. In all cases, the targets were polished, cleaned, and mounted in the target test chamber under a vacuum of approximately 10^{-6} torr. Each target was then irradiated with the laser in the Q-switched mode, imparting an energy on target from 2 - 6 joules. The laser interacts with the surface causing melting and vaporization of target material in the vicinity of the impact area and producing a hot, dense expanding plasma over the target surface. After laser plasma exposure, the targets were inspected by optical and scanning electron microscopy to evaluate the effects of laser-plasma exposure in general and the suscep-tibility of the target material to unipolar arcing damage in particular.

A. CONDUCTORS

1. Type 304 Stainless Steel

The main laser impact crater measured 1.15 mm in diameter with a depth of approximately 50 μm. The plasma damaged surface area has a diameter of 2.5-3.0 mm, extending radially approximately 0.9 mm beyond the laser impact area. Figure 15 is a photograph taken by scanning electron microscope (SEM) of the main crater. This figure shows the molten appearance of the sample immediately surrounding the main crater due to the longer duration of the energetic plasma contact with the surface and the concentration of the plasma energy at the surface due to unipolar arcing. Figure 16 is a SEM view of the perimeter of the main laser crater area where the damage mechanism transitions from combined laser/plasma surface interaction to strictly expanding plasma-surface interactions. This view shows the high density of unipolar arc craters immediately surrounding the laser impact crater. From this view it can be easily seen that the number density and size of the unipolar arc craters decreases radially from the impact crater. This indicates that the duration or burn time of the unipolar arcs decreases as the expanding plasma cools, until at a radial distance of approximately 3 mm there is no more evidence of arc initiation. Figure 17 shows a SEM view of unipolar arc damage just beyond the laser impact crater.

45
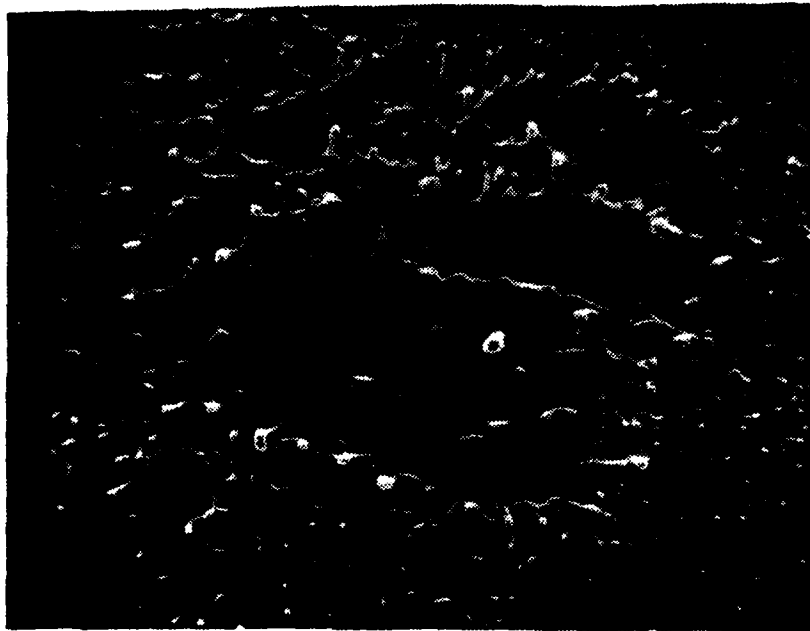
Figure 15.   Type 304 stainless steel.   Laser impact area
             (65 X SEM).

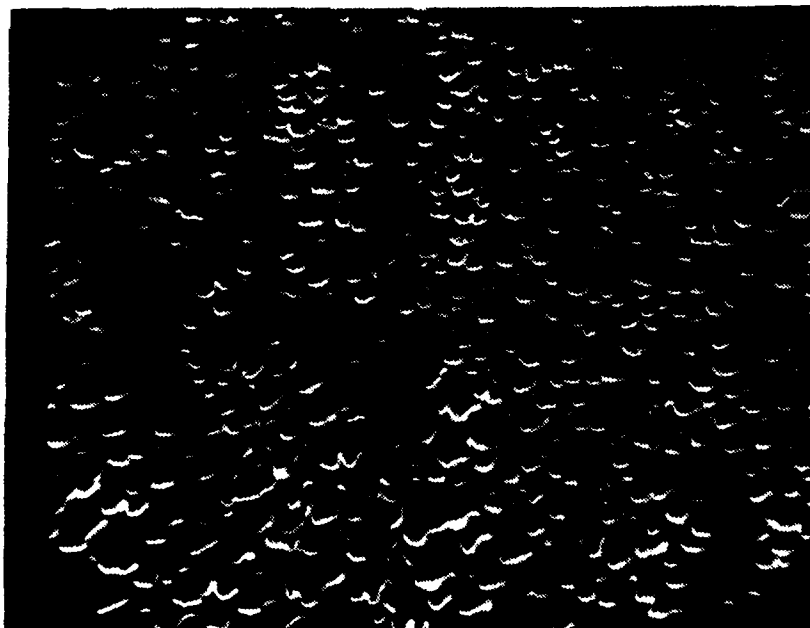Figure 16.   Type 304 stainless steel.   View of area just
             outside laser impact crater (toward bottom)
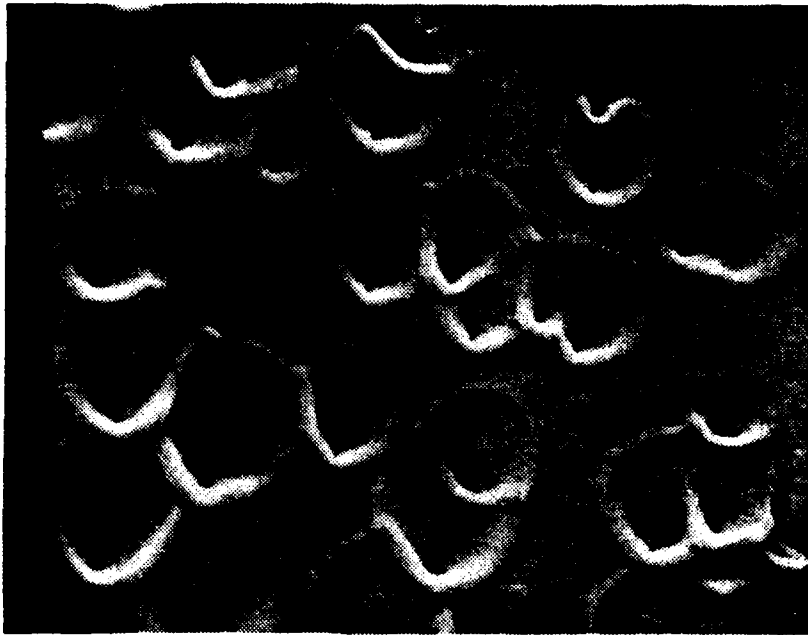   (250 X SEM).

Figure 17.   Type 304 stainless steel.   Overlapping unipolar
             arc craters just outside laser impact area
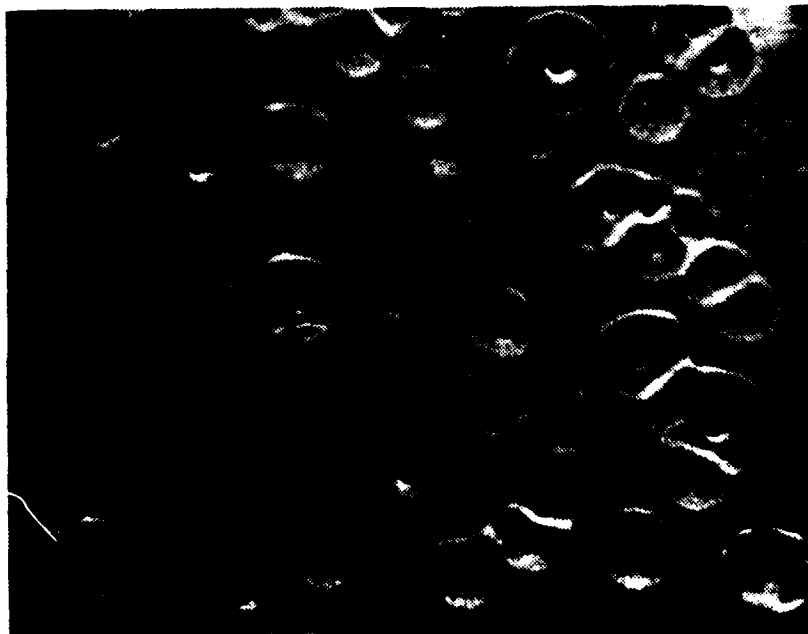   (1300 X SEM).

Figure 18.   Type 304 stainless steel.   Unipolar arc craters
             outside molten region.   (1300 X SEM).

The oblong, spread out appearance of the craters indicates that in this region the surface was molten while the arcs were in progress. Figure 18 shows the unipolar arc damage in an area radially further out from the center of the main impact crater, a distance of 1.2 mm. Even this far from the laser-surface interaction area, there is an extremely high arc density of about 6×10^5 arcs per square centimeter. The craters with large diameter rims of 15-20 μm correspond to ones with the longest arc duration, while those initiated later in the plasma-surface interaction are smaller, having rim diameters of 5-10 μm. Most of the craters have a hemispherical shape surrounded by a pronounced rim with a small dark spot of 1-2 μm in size in the crater center. These dark spots are the cathode spots and are cylindrical in shape with a depth of 3-6 μm. The hemispherical crater and rim are formed by the localized melting in the area surrounding the cathode spot and the outflow of molten metal caused by radial plasma pressure.

The type 304 stainless steel sample exhibited a high density of unipolar arcs over a diameter of about 3 mm, indicating it has a high susceptibility to arc initiation. Outside 1.0 mm from the center of the laser impact area there was no more whole area surface melting. Craters caused by unipolar arcing were the only damage mechanism in this area.

48

2. Spectrally Pure (.9999) Aluminum

For this experiment, spectrally pure billets of aluminum (melting temperature 660°c) were purchased to evaluate unipolar arcing on the pure metal rather than an alloyed aluminum used for structural purposes. The main laser impact crater measured 1.7 mm in diameter with a depth of about 70-80 μm. Outside this area, the area of plasma-surface interaction is an annular ring of 0.6 mm thickness. The total diameter of the damage area is 3 mm, the same as observed in the stainless steel specimens. Figure 19 is a SEM photograph of the main laser impact crater. The main damage crater on the aluminum sample measures 0.55 mm larger than the impact crater on stainless steel. However, the molten area due to hot laser-plasma interaction does not extend as far out from the center of the laser impact area as in stainless steel. This may be due to the fact that the pure aluminum has a very high value of thermal conductivity (238 W/mk) as compared with stainless steel (40 W/mk). Figures 20 and 21 are SEM photographs of the transition area from laser impact to solely plasma inter-action. The boundary is much more distinct in aluminum with the unipolar arc craters close in to the impact crater showing none of the flow deformation experienced with stainless steel. The unipolar arc craters decrease in density and crater diameter as the radial distance from the
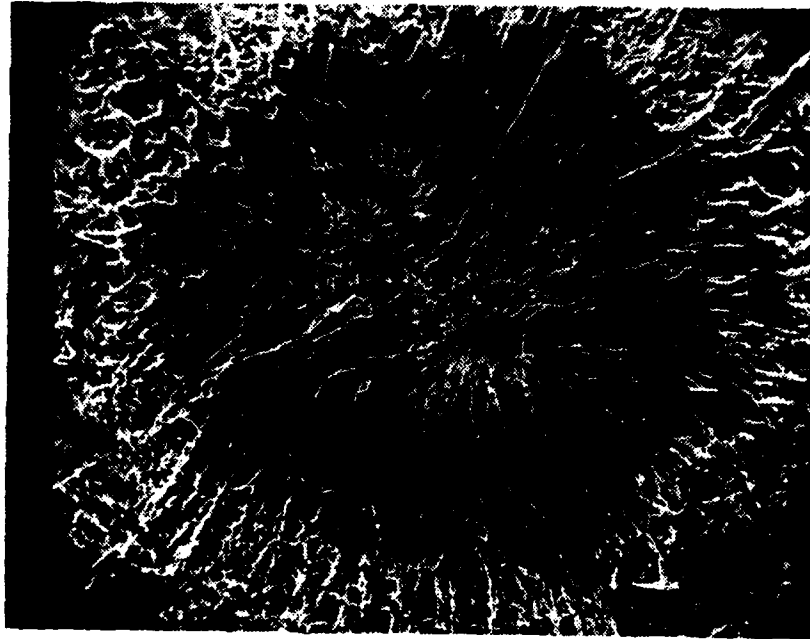
Figure 19. Spectrally pure aluminum. SEM view of laser impact area. (65X SEM)
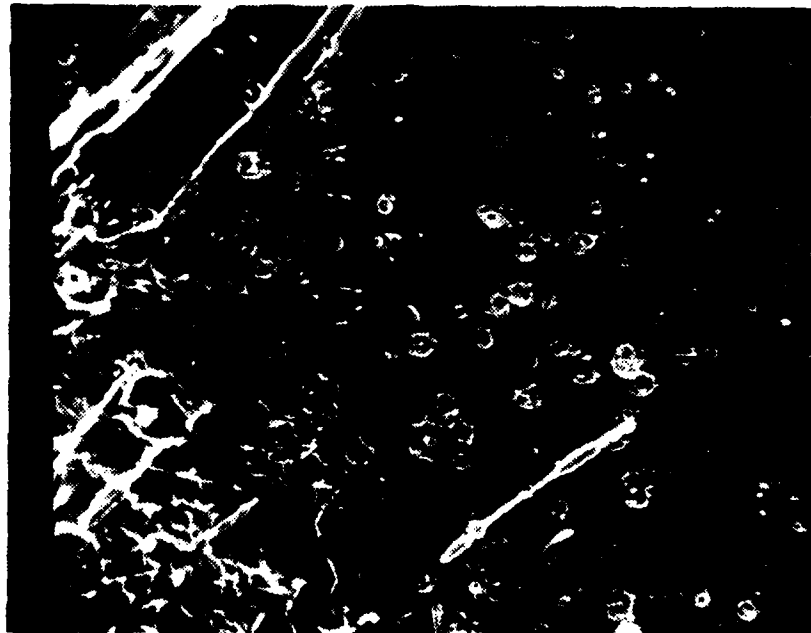

Figure 20. Spectrally pure aluminum. Transition from laser impact area to plasma-surface interaction zone. (250X SEM)
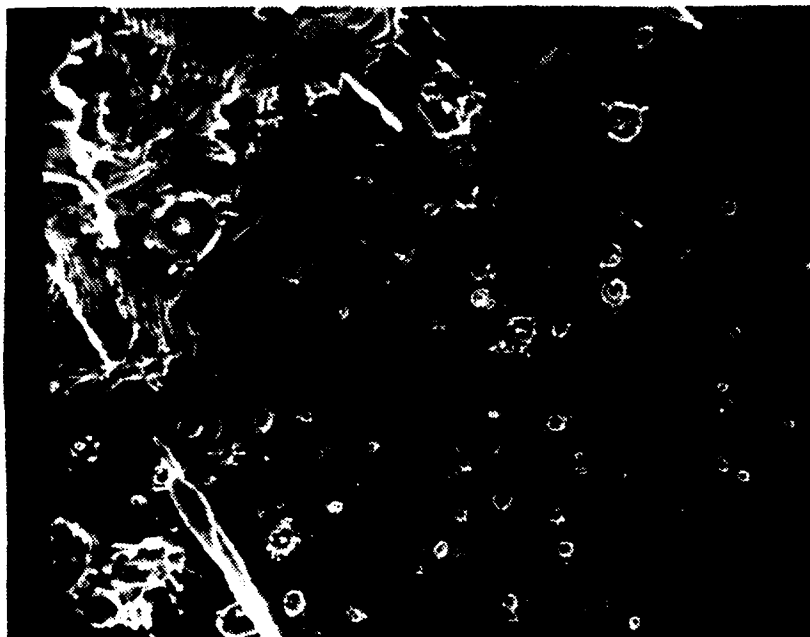
Figure 21.   Spectrally pure aluminum.   Different view of
transition area from impact crater to plasma
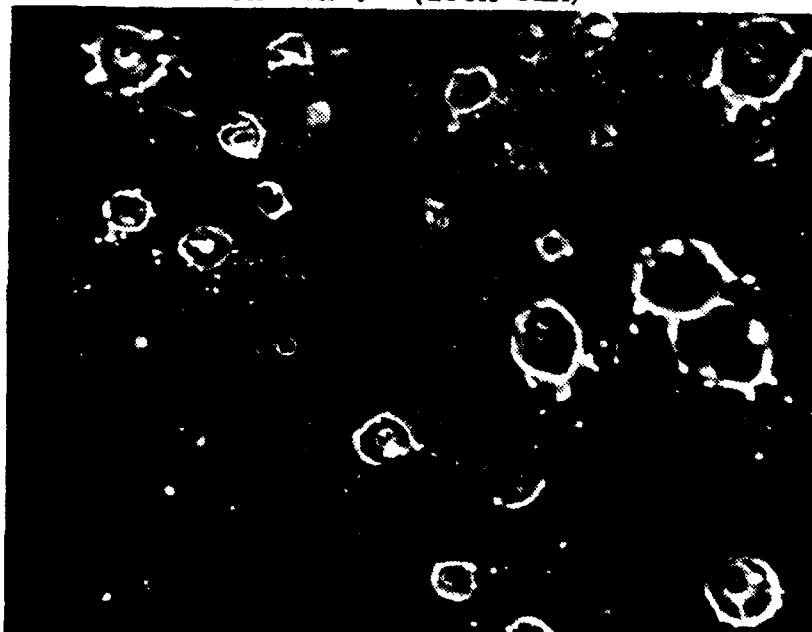interaction zone.   (250X SEM)

Figure 22.   Spectrally pure aluminum.   Outside laser impact
area.   Unipolar arcing only damage mechanism in
this area.   (1300X SEM)

impact crater center increases. The arc craters have the same general shape and cathode spots as experienced in stainless steel, but the crater rims are much sharper and more distinct, indicating that the unipolar arcs were sustained after the base metal had solidified or were radially further out where there was no surface melting of the aluminum target. Figure 22 shows a SEM view of unipolar arc craters in the plasma-surface interaction zone. The arc density was about 5×10^5 arcs per square centimeter with crater diameters ranging from 2-10 μm. The smaller, more sharply defined arc craters indicate that the arc current causes less localized melting and subsequent outflow of material than experienced with stainless steel samples due to the much larger heat conduction in aluminum. This is consistent with the results noted for the laser impact crater area.

3. Molybdenum

The main laser damage crater on the molybdenum sample measured 0.9 mm in diameter which was smaller than for the stainless steel or aluminum. Also, the plasma-surface interaction zone had a measured diameter of about 2.0 mm which is also smaller than for the other samples. One possible explanation for this is that molybdenum has a much higher melting temperature (2615°C) than even stainless steel (1536°C), and, as a result, the laser surface interaction may produce less melting and evaporation of target

material for molybdenum. Also, a smaller radius of unipolar arcing damage was observed in molybdenum compared to stainless steel. Figure 23 is a photograph of the transition from laser impact area to the surrounding area of plasma-surface interaction. This figure shows a fairly high unipolar arc density with the appearance of the craters being smoothed over somewhat by the molten surface effects. Figure 25 is a SEM view of unipolar arc craters close in to the laser impact area. This figure shows the smoothing effect due to the flow of molten metal at the surface layer. It would appear that most of the arcing in this region occurred before or during the solidification process. Figure 26 shows unipolar arc craters formed outside the area of molten flow. These craters have the expected shape with diameters measuring 6.0-12 μm and were formed on the base metal outside the molten area.

    4. Nickel

A polished nickel specimen was chosen for investigation primarily because the previous study by Barker and Rush [18] reported that nickel did not show any evidence of unipolar arcing when exposed to a laser-induced plasma. However, the metallic properties of nickel such as electrical conductivity, thermal conductivity (88.5 W/mk), and melting point (1455° C) fall in the same general range as other materials which arc easily.
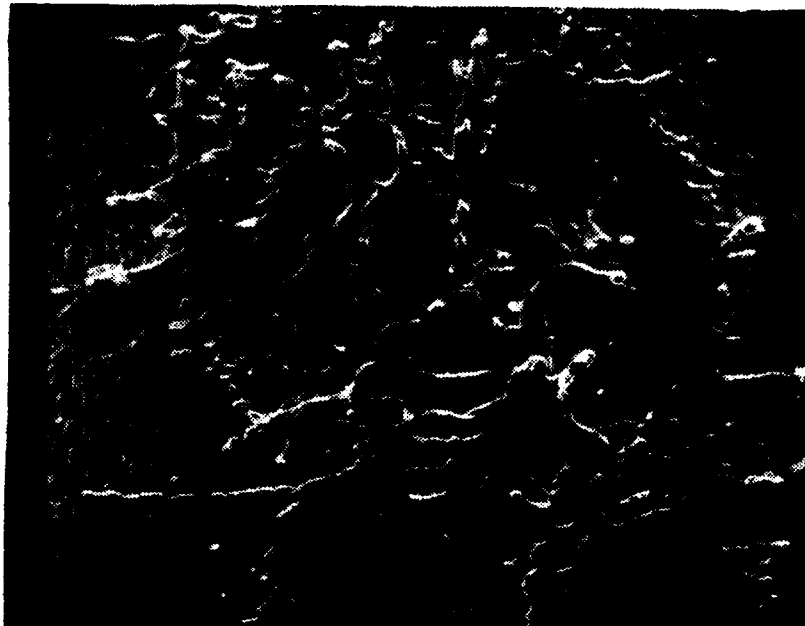
Figure 23. Molybdenum. Main Laser Impact Crater (110X SEM)
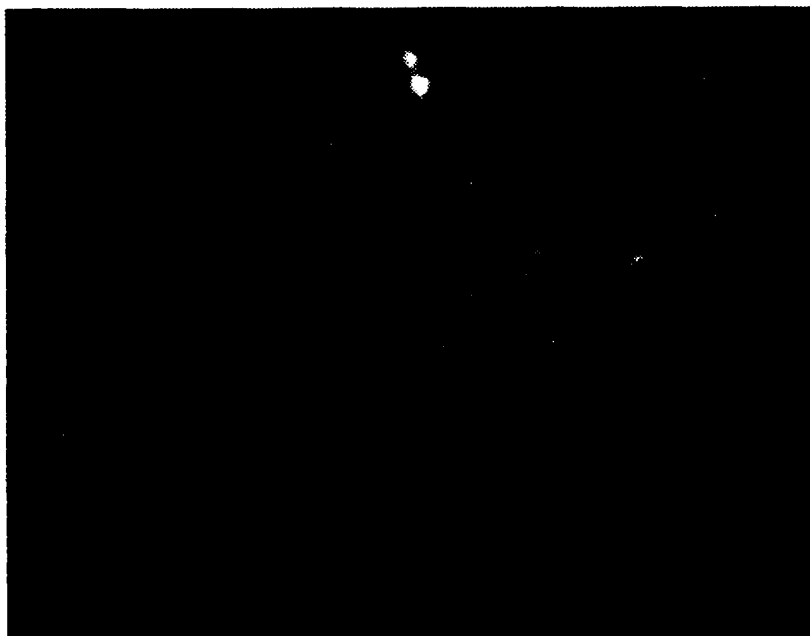

Figure 24. Molybdenum. Transition from Laser impact area
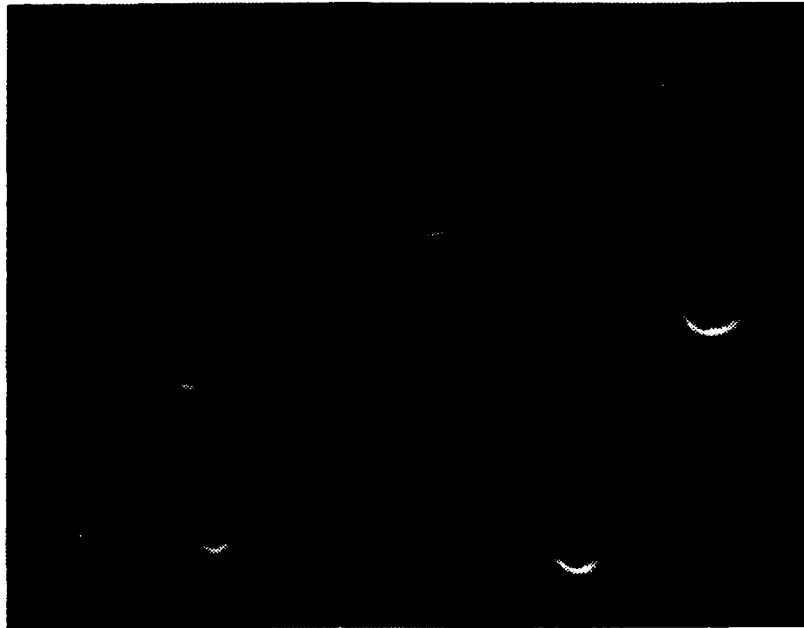to area of plasma-surface interaction.

Figure 25.   Molybdenum.   Unipolar Arc Craters formed in
Molten Area.   (1100X SEM)

Figure 26.   Molybdenum.   Unipolar Arc Craters outside
Molten Area.   (1100X SEM)

The main laser impact crater measured 1.6 mm in diameter
which is similar to that of aluminum and larger than that
of stainless steel. The main difference, however, was that
the molten area surrounding the impact crater formed an
annular ring of 0.75 mm in width. This gives an overall
laser damage-molten area diameter of 3.1 mm which is larger
than the overall plasma-surface interaction diameter
observed in aluminum or steel. Figure 27 is a photograph
of the extreme edge of the primary damage area transition-
ing into an area that has experienced surface melting and
smoothing. The implication is that the area of surface
melting for nickel is greater than the area that would be
anticipated for unipolar arcing damage to the target
surface. This means that when arcing takes place, the
material is in a molten state and will reflow over the
cathode spot after the arc ceases if the surface layer is
still molten. Only those arcs that are initiated late in
the cycle would then leave craters on the surface.
Figure 28 shows a molten area about 2 mm from the center
of the laser impact area that appears to have many arc
craters that have been deformed and smoothed by molten flow
after arc cessation. Figure 29 shows unipolar arc craters
at the very edge of the plasma-surface interaction area
about 3.0 mm from the center of the laser impact crater.
Even this far from the laser crater, the arc rims are barely
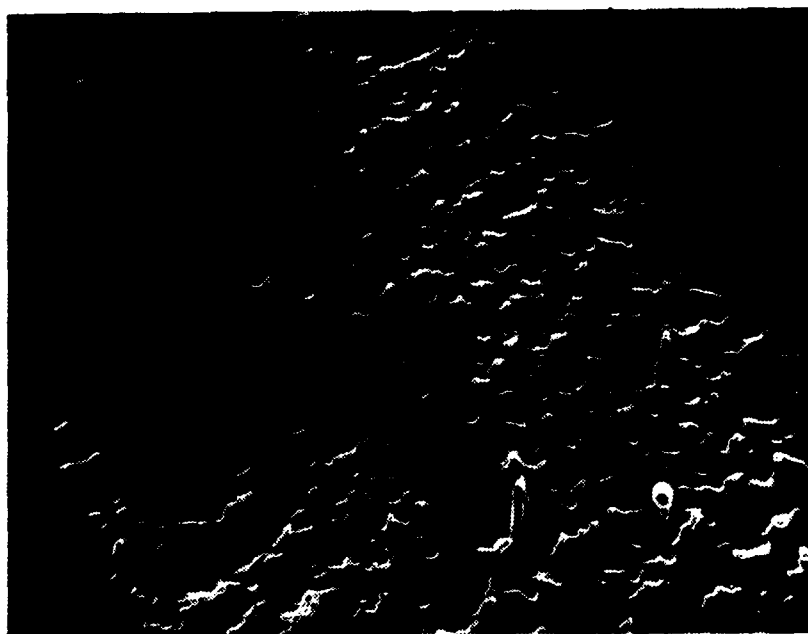
56

Figure 27. Nickel. Transition from Laser Impact Area
            (lower photo) into smoothed over area of
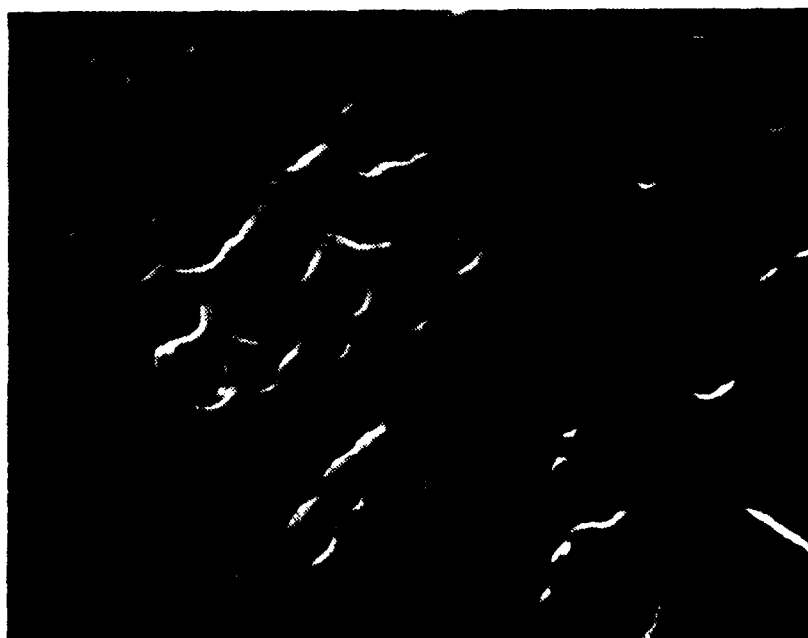   surface melting.   (200X SEM)

Figure 28. Nickel. Molten area at edge of primary damage
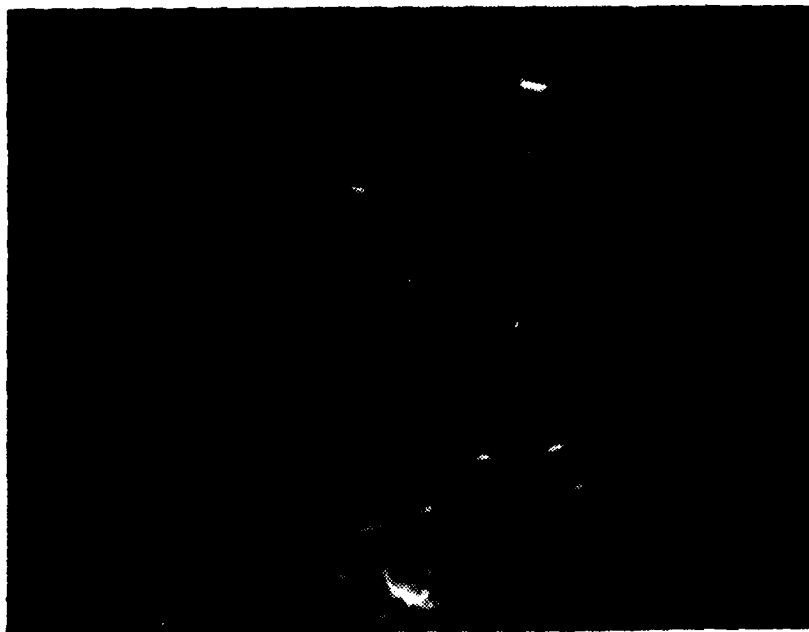   area.   (1000X SEM)

Figure 29. Nickel. Unipolar arc craters at extreme edge
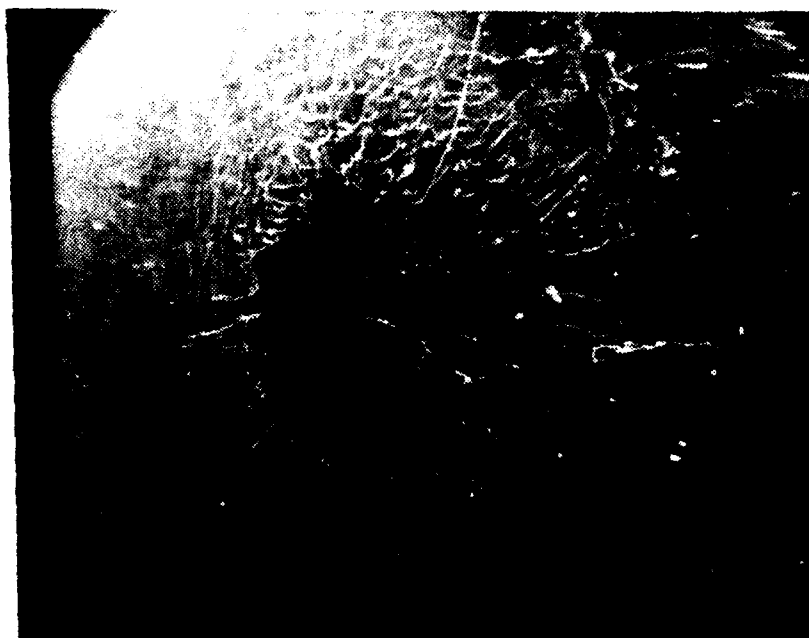of plasma-surface interaction area. (2000X SEM)

Figure 30. Silicon. Main laser impact crater. (25X SEM)

discernible on some of the older craters which have been smoothed by the reflow of molten material.

It would appear that nickel is, in fact, susceptible to unipolar arcing, but the craters which normally serve as evidence are smoothed over by the still molten surface layer.

B. SEMICONDUCTORS

Two semiconductors, silicon and germanium, were chosen to investigate the widespread assumption that unipolar arcing requires not only a hot dense plasma, but that the plasma be in contact with a highly conducting surface. Both semiconductors chosen have similar metallic properties as the previously investigated conductors with the main difference being that the electrical resistivity of silicon is five to six orders of magnitude greater than that for the conducting metals and that for germanium it is about four orders of magnitude higher. It is suspected that this higher resistivity will prevent or greatly reduce the ability of the sheath potential to provide enough driving force to sustain a current loop of the required magnitude within the material for unipolar arcing to occur.

1. Silicon

The main laser impact area has a diameter of 2.0 mm and shows the same pattern of melting and evaporation as observed on conducting materials. By photographing the

59

light flash emitted from the laser produced plasma, it was
possible to verify that a hot, dense silicon plasma was
produced. Figure 30 is a photograph of the main laser
impact area showing the melting and splattering of material
removed from the impact crater. Figure 31 is a SEM view of
the molten center of the laser impact area. The only
distinctive feature of the silicon in this area is the
pattern of stress fractures over the surface. Silicon,
being very brittle, produces high enough stresses during
the rapid cooling of the molten surface layer to produce
this pattern of fractures to relieve the induced stresses.
Figure 32 is a view of the transition from laser impact area
to the plasma-surface interaction area. From this picture
it can be seen that the surface melting extended only about
0.25 mm beyond the main splatter area. There are ridges
and surface fractures in this view but no evidence of
unipolar arcs. Figure 33 is a magnified view of the same
area. Once again, no evidence of unipolar arcing was
observed.

It would appear that the high resistivity of silicon
compared with that of conducting metals is enough to prevent
the initiation of unipolar arcing. In silicon, the smaller
area of surface melting is due to the even flow of ions and
electrons to the surface and their recombination there. In
contrast, large surface melting areas are observed for
conductors when unipolar arcing occurs. This implies that

more of the available plasma energy is deposited on the surface when arcing occurs.

2. Germanium

A germanium target was also chosen since its electrical resistivity is less than that of silicon by a factor of about 10. This, however, is still three orders of magnitude higher than the resistivity of conducting metals. The main laser impact crater measured 2 mm in diameter and has the same pattern of surface melting and stress fractures as silicon. Figure 34 shows the main laser impact crater and figure 35 is a view of the center of the main crater showing the stress fractures caused by the rapid cooling. Figure 36 shows the outer perimeter of the main crater with no evidence of unipolar arcing. It appears that there exists a maximum resistivity of the exposed surface material to support unipolar arcing that lies somewhere between that of stainless steel (70 $\mu\Omega/cm$) and that of germanium (89×10^3 $\mu\Omega/cm$).

C. METALLIC GLASSES

In this section of the experiment, three different alloys of metallic glasses provided by Professor Wagner at UCLA were subjected to a laser-induced plasma to determine their susceptibility to unipolar arcing. Before reviewing the results of the experiments, a short discussion follows on the structure and properties of metallic glasses in general.
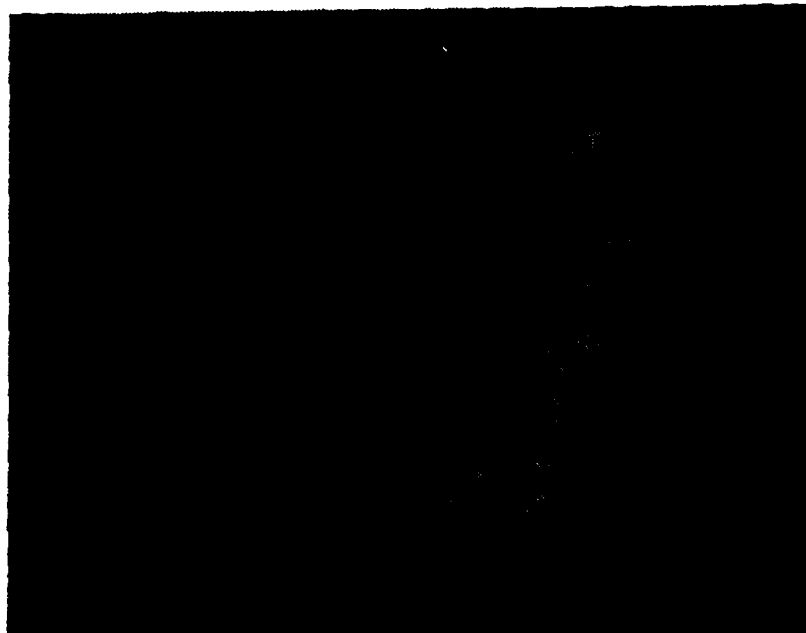
61

Figure 31. Silicon. Molten center of laser impact crater.
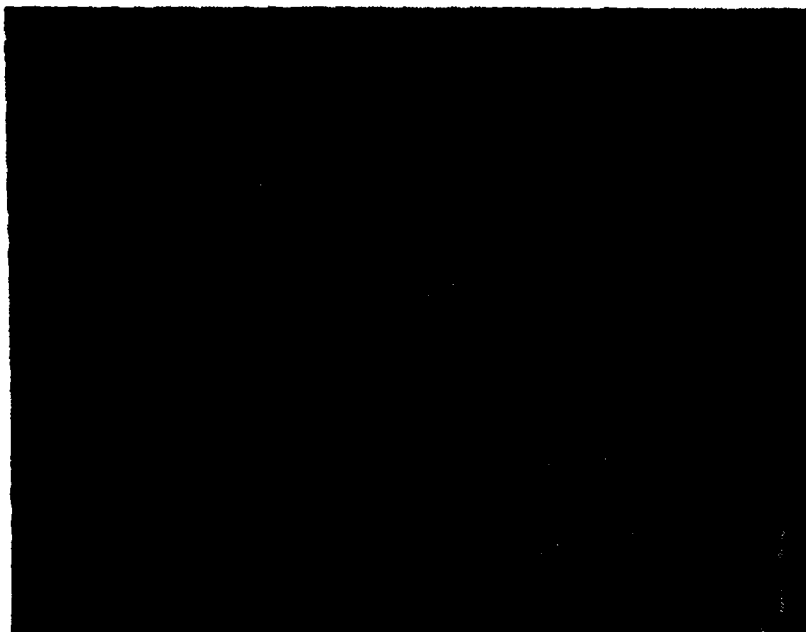(400X SEM)

Figure 32. Silicon. Edge of laser impact area (bottom
photo) and surrounding area exposed to plasma.
(400X SEM)

Figure 33.   Silicon.   Different view of perimeter of main
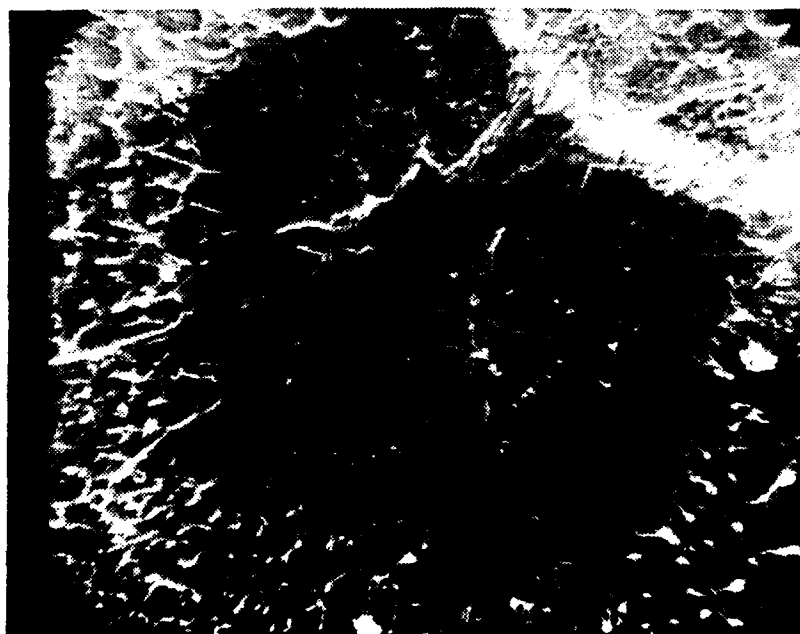crater.   (630X SEM)

Figure 34.   Germanium.   Main laser impact crater.   (50X SEM)

Figure 35.   Germanium.   Stress fractures at center of laser
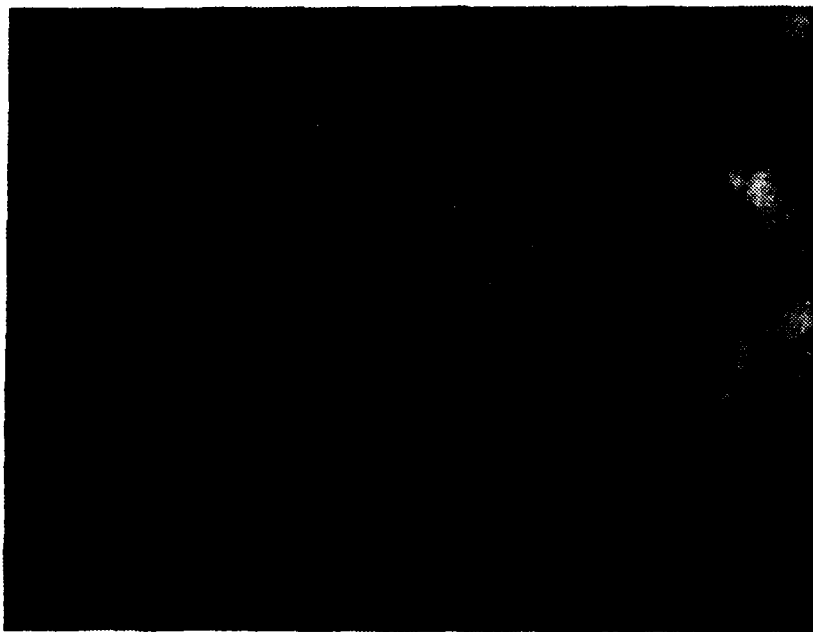impact area.   (400X SEM)

Figure 36.   Germanium.   Outer perimeter of main crater.
(1000X SEM)

Usually when a liquid freezes, the atoms or molecules come to rest only after taking up positions in an orderly array: a crystal. In the formation of a glass, on the other hand, the atoms of the liquid essentially stop in their tracks. Therefore, the configuration of atoms in the glass is very much different from that of a normal crystalline solid. For a glassy material to form it must be cooled to a temperature below a certain threshold called the glass temperature. Above the glass temperature the atoms are free to make transitional movements while below that temperature, they are immobilized except for vibrational motions about their average positions [19] . The reason metallic glasses were initially difficult to produce is that the glass temperature of metals lies well below the freezing point where crystallization takes place. The strategy for creating a metallic glass is to cool the liquid metal rapidly from above the liquidus temperature to below the glass temperature. If the passage through the intervening region is fast enough, there will not be time for crystals to form. Metals, on the other hand, form low viscosity liquids that very rapidly crystallize. Quenching rates in excess of 10^{10} degrees centigrade per second are needed to convert pure metals into glasses. However, alloys of metallic glass require much lower rates on the order of 10^5-10^6 degrees centigrade per second [20] . Although the crystalline state is favored thermodynamically, metallic

glasses are stable below a certain temperature called the devitrification temperature (approximately 700° F for steel alloys).

Most metallic glasses are produced by spraying a thin jet of molten metal onto the surface of a rotating metal disc or cylinder which is held at room temperature. This process is called direct quench casting and it is a very economical process for producing metallic glass. The only difficulty with this method is that it only produces narrow ribbons of metallic glass such as were used in this experiment. New methods of laser glazing are being investigated to produce sheets of metallic glass-coated metals [21] .

Many properties of a metallic glass such as density, heat capacity, and compressibility hardly differ from those of a crystalline metal with the same composition. However, the lack of long range order and grain boundaries lead to some other remarkably differing properties. Metallic glasses, in general, are ductile and in tension are among the strongest of all alloys. The lack of grain boundaries to act as sites for chemical attack makes metallic glasses very corrosion resistant. Finally, all resistance to the flow of electric current in a metal results from irregularities in the periodic arrangement of the atoms in a solid. Because metallic glass have extensive disorder built into their structure, they tend to have a high resistivity, typically an order of magnitude higher than the same

66

material in crystalline form [19] . It is this higher
resistivity that indicates metallic glasses might be some-
what resistant to unipolar arc damage.

1.   Metallic Glass Number One   (Nickel 35, Zirconium 60,
                                   Cobalt 5)

The main laser crater measured 1.5 mm in diameter
and showed much less of a splattered appearance than the
impact craters of the previous experiments on pure metals.
Figures 37 and 38 are optical microscope views of a portion
of the main crater and the area surrounding the perimeter
of the crater. There is significant melting in the crater
area, but there seems to be much less flow of material from
the crater center in a radial direction. Figure 39 is a
photograph of the center of the main crater. There is
significant melting, as expected, but no sign of unipolar
arc craters. Figure 40 is an optical microscope view of the
target surface just outside the main crater perimeter. The
craters in this photograph are 10-20 μm in diameter and
have the same shape and size expected for unipolar arcs.
The smoothness of the crater rims indicate that the surface
area was molten during the arc lifetime. The density of arc
craters in the plasma-surface interaction area is very low
and appears localized in areas on the periphery of the
impact crater.

Figure 37. Metallic Glass Number One. View of main crater
center (bottom of photo) and perimeter area.
(100X optical)

Figure 38. Metallic Glass Number One. View of perimeter
of main laser crater. (100X optical)

Figure 39.   Metallic Glass Number One.   Center of main
             impact crater.   (200X SEM)

Figure 40.   Metallic Glass Number One.   Perimeter outside
             main laser impact crater (to left of photo).
             (100X optical)

2. <u>Metallic Glass Number Two</u> (Titanium 50, Nickel 45, Zirconium 5)

The main laser impact crater on this specimen was about 1.8 mm in diameter with the same pattern of melting without appearing to splatter as was observed in METGLAS number one. Figure 41 is an optical microscope view of the outer perimeter of the main crater showing the pattern of flow of the molten material. Figure 42 is another photograph of the same area at higher magnification that shows no sign of unipolar arc damage. Figure 43 is a SEM view in the crater area. The spheroid shaped particles seem to be globules of molten material that settled back in the crater area. The fact that they appear to be glowing indicates that they are not actually connected to the surface and as a result are collecting the electrons from the scanning electron microscope and building up a charge. Figure 44 is an optical microscope picture of localized, low density (100 per cm^2) unipolar arc craters outside the main laser crater. The arc crater diameters range from 5-20 μm and have the same appearance as the craters observed on METGLAS number one.

3. <u>Metallic Glass Number Three</u> (Nickel 35, Titanium 65)

The main laser impact crater had approximately the same diameter and appearance as METGLAS number two which is not surprising considering the similarity of their respective compositions. Figures 45 and 46 are photographs of
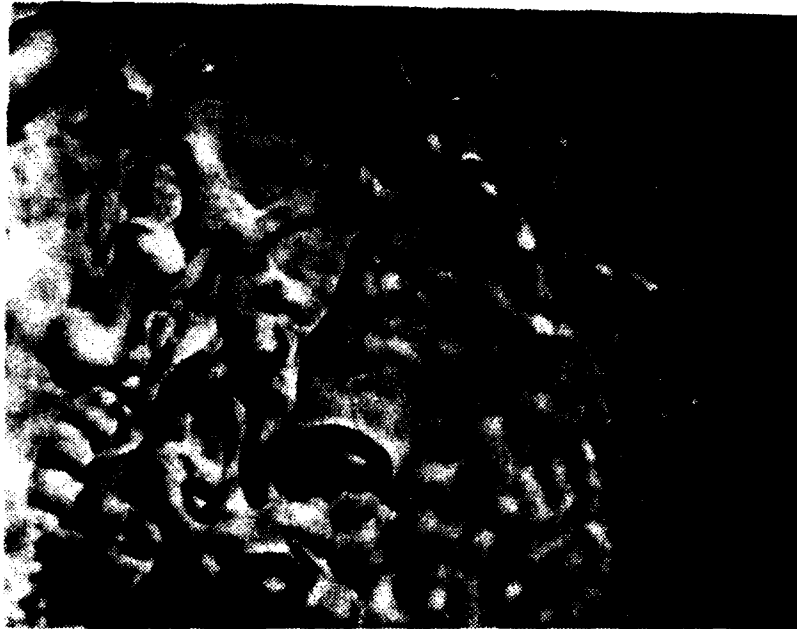
70

Figure 41.   Metallic Glass Number Two.   Outer perimeter of
             main crater (right photo).   (100X optical)

Figure 42.   Metallic Glass Number Two.   View of main crater
             center.   (200X optical)

71

Figure 43.   Metallic Glass Number Two.   SEM view of main
             crater center.   (1000X SEM)

Figure 44.   Metallic Glass Number Two.   Localized unipolar
             arc craters outside main laser crater.
             (400X optical)

the solidified globules of molten material in the laser impact area. Figure 47 is an optical microscope view of what appear to be low density unipolar arc craters just beyond the main laser crater melt area. The crater diameters have the same 5-20 μm range as was observed in METGLAS number two.

4. Comments on Metallic Glasses

All three of the metallic glass alloys showed a high resistance to unipolar arc damage. In addition, the area of surface melting for each of the metallic glasses was smaller than for the conductors and semiconductors evaluated previously. The metallic glasses appear overall to be more resistant to laser-surface interaction damage and plasma-surface interaction damage.

Figure 45.   Metallic Glass Number Three.   Main laser impact
area.   (200X SEM)

Figure 46.   Metallic Glass Number Three.   Main laser impact
area.   (1000X SEM)

Figure 47. Metallic Glass Number Three. Unipolar arc
damage beyond perimeter of main crater (to
left of photo). (400X optical)

V. ARC INITIATION

In arc physics the Fowler-Nordheim theory [22, 23] predicts the theoretical value of electron current as a function of the average electric field. In practice, the current is greater than the theory predicts. To explain this it is usually assumed that microscopic protrusions on the cathode surface locally enhance the field and that the emission originates at these surface features [24 - 27] . Several experiments have been done to investigate the role of contaminents and microroughness of the surface as a factor in arc initiation, either vacuum arc or unipolar arc [10, 14, 28] . The experimental results show conclusively that these surface features do act as arc initiation sites as the theory predicts. Clean, highly-polished surfaces on the other hand permit arc initiation without these microscopic field enhancement features.

A. MICROWHISKERS

Local electric field enhancement must happen even on clean, highly-polished metal surfaces if arcing is to occur. Vibrans has completed an analysis to determine the minimum size microscopic protrusion or microwhisker needed to give the required field enhancement for arcing. As an example: clean polished copper with a work function of 4.5 eV was used. Assuming a hemispherically capped cylindrically shaped microwhisker, a Fowler-Nordheim analysis would

76

require a microwhisker 2.1 μm high and 0.016 μm in diameter [29] .

Several investigators have searched for these micro-whiskers on polished surfaces. Using scanning electron microscopy with resolution down to 10^{-8}m they were unable to detect protrusions which could account for the observed electron emission [28, 30] .

At this point, assuming that the required field enhancement is a surface feature, three proposals can be made:

1. The microwhiskers lie down during the polishing process and are therefore not visible under the microscope. When an electric field is applied they pop up to provide the arc initiation site.

2. The microwhiskers are smaller than 10^{-8}m but with some irregular geometry, not considered by Vibrans, still capable of providing the field enhancement.

3. Some other surface feature such as grain boundaries provide the electric field enhancement at the arc initiation sites.

A new experiment has been devised and performed to show conclusively that microwhiskers are not necessarily required for unipolar arc initiation on polished metal surfaces.

Using the experimental set up described in section III it is possible to create metallic glass on the surface of

AISI 304 stainless steel targets [20, 21, 31]. Basically, the metallic glass is formed by melting a thin surface layer of the material with the high power laser then letting it solidify at a very high cooling rate. This leaves the material in an amorphous rather than crystalline state. The base metal acts as a heat sink providing the rapid cooling of the thin liquid film. Metallic glass has very good anticorrosive properties so that when the target is etched the metallic glass becomes clearly evident. Figures 48 - 57 show the results of this procedure. The dark areas are the metallic glass and the lighter areas are the base metal which have been etched away. In figure 48 taken with an optical microscope, the darker areas are the base metal. Here the grain boundaries of the base metal can be seen.

The required cooling rate is inversely proportional to the thickness of the metallic glass film. In those areas in which metallic glass is formed without the coincident formation of a plasma (lower energy density areas) the surface remains polished. The time required to form the metallic glass is less than the time required for the molten metal to flow. To get an appreciation for the time required to form this layer we first must consider the thickness of the layer which is in turn a function of the laser skin depth on this particular material. To determine the skin depth a solution to the general wave equation must be found. The application of the Fresnel equations must then be completed

for the laser surface interaction. However, an approximate relation will be sufficient for this discussion. The skin depth is approximately [32] :

$$\delta = \sqrt{\frac{\rho}{\pi \mu \nu}}$$

where δ is the skin depth or depth at which both the E and H vectors of the incident radiation fall to 1/e of their surface values. ρ is the resistivity of the target material, μ the target permeability and ν the laser frequency. For the Nd-YAG laser striking AISI 304 stainless steel:

$$\rho = 700 \ \mu\Omega/mm = 0.7 \ \Omega/m$$
$$\nu = 3 \times 10^{14} \ HZ$$
$$\mu = 1$$

which gives a skin depth of $2.6 \times 10^{-8}m$ or 260 Å. The depth of a unipolar arc crater is 3-6 μm or 100 times deeper than the depth of the metallic glass layer. Figure 60 confirms the thin film nature of the metallic glass layer. The target was etched after the arcing occurred on the metallic glass. The etchant has eaten away the base metal in the arc spot leaving the thin metallic glass layer around the arc spot.

For laser produced metallic glass, quench rates on the order of 10^8 deg.C/sec have reported for layers 1-10 μm deep [31] . Our layer is even thinner than this so that even higher quench rates are likely. The laser delivers sufficient energy to the target surface to melt some areas. As soon as the energy deposition ceases the quenching commences and the metallic glass is formed within tens of nanoseconds and certainly within a few hundred nanoseconds.

In general breakdown occurs early in the laser pulse and a plasma is produced. Only the first part of the laser pulse goes to form the metallic glass. As soon as the plasma is formed it cuts off the laser energy deposition on the surface. The later half of the laser pulse goes into heating the plasma. If we reduce the laser pulse energy below that required to form a plasma we can still form the metallic glass. Since the entire pulse is now deposited on the target surface we are using about the same amount of energy to form the metallic glass. This experiment was done. The laser energy density on the target was reduced. The lack of a plasma was confirmed by photography and we observed essentially the same metallic glass pattern on the target surface as we have seen on the targets on which a plasma was produced and arcing occurred.

The metallic glass is completely formed before the unipolar arcing occurs. The time estimates above support this. We also have some experimental evidence that the

unipolar arcing occurs only after the metallic glass has been completely formed. If arcing were occurring either before or during the formation of the metallic glass additional heat energy from the arcing would be added to that from the laser to form larger areas of metallic glass. The metallic glass islands would swell in areas of unipolar arc craters and diminish in areas of no craters. The boundaries of the metallic glass islands would be affected by the location of the arc craters. In figures 52, 53, 56, 57 it is clear that this is not the case. The shape of the metallic glass islands is not in any way affected by the location of the unipolar arc craters. The metallic glass is formed prior to unipolar arcing on the surface.

Perhaps the most important observation of this section is the fact that during the formation of the metallic glass any microwhiskers lying down or smaller than 10^{-8}m would have been vaporized or melted. The fact that arc craters are seen in the metallic glass is evident that microwhiskers are not required for arc initiation.

At this point an obvious question arises: Why do the metallic glass areas arc at all? When we did experiments with commercially prepared metallic glass we found that very little arcing occurred in the presence of a self-consistent plasma. Now we see that unipolar arcing has a propensity to arc on the metallic glass when it is formed as a thin film on a metal surface, see figures 49-51.
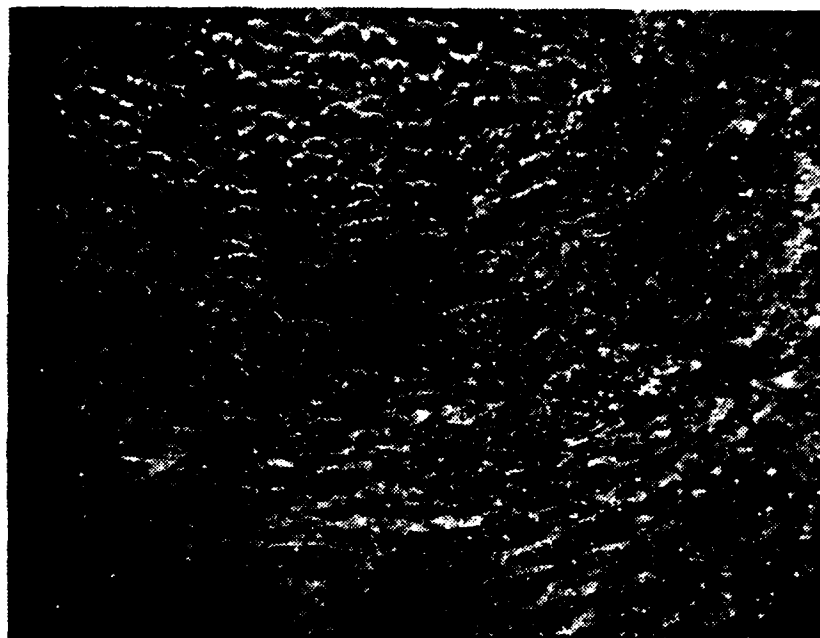
Figure 48. AISI 304 stainless, irradiated then etched, SEM 65X, Laser Impact area at top.
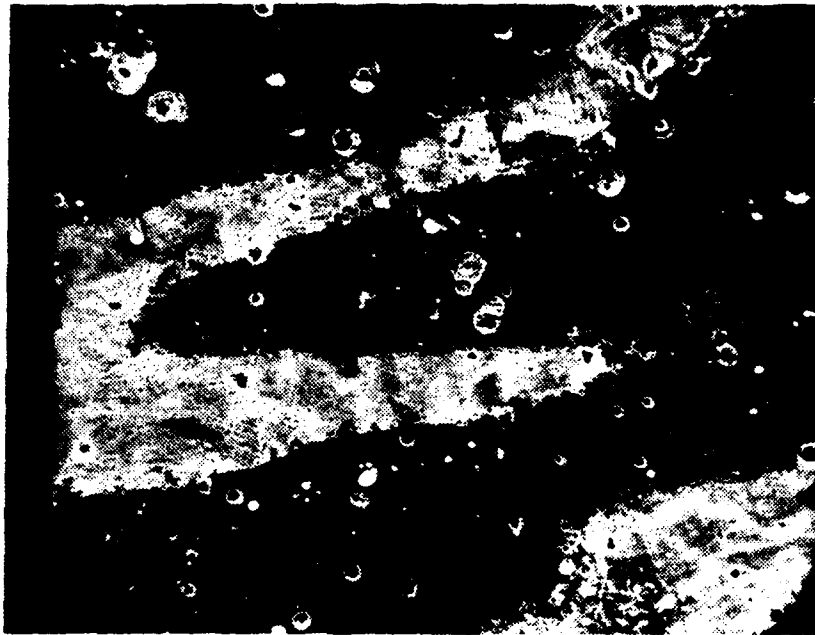

Figure 49. Same as above, 130X.

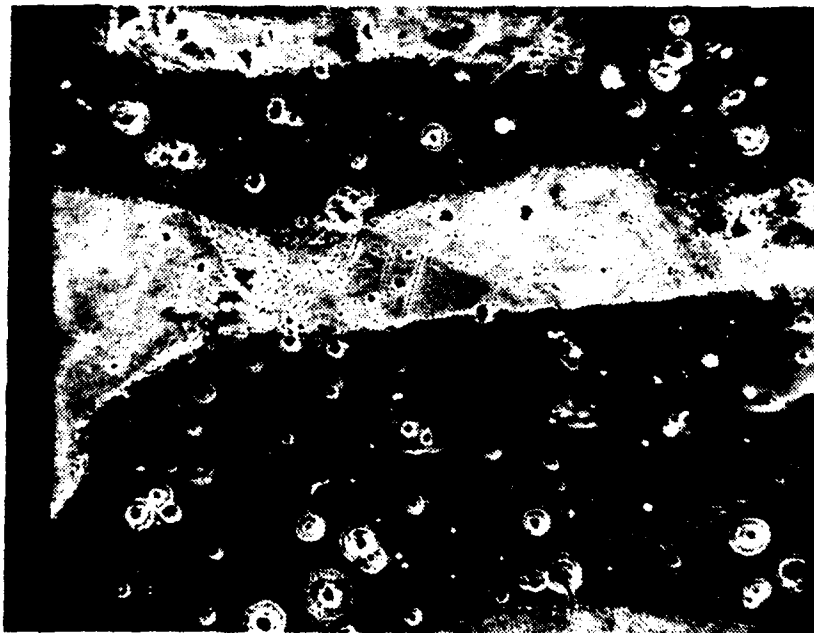Figure 50.   AISI 304 stainless irradiated then etched,
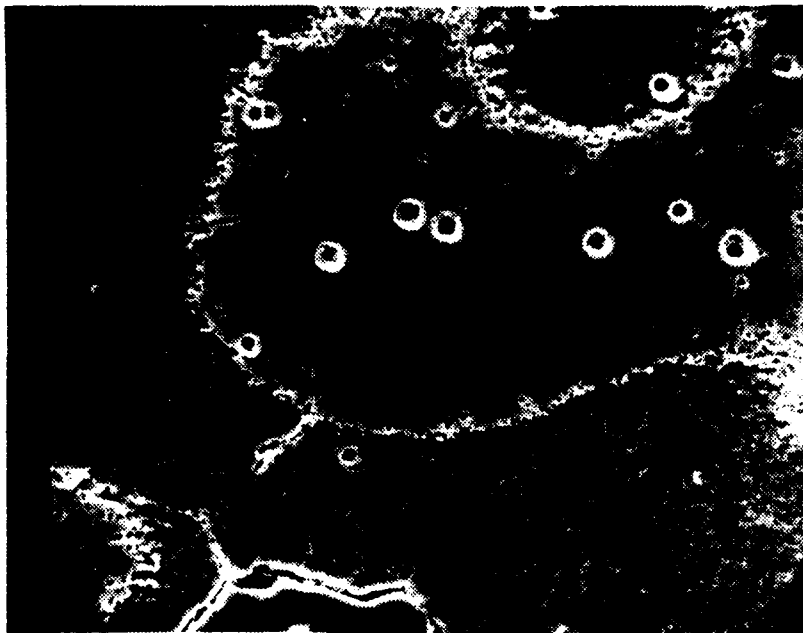SEM 650X.

Figure 51.   Same as above.

83

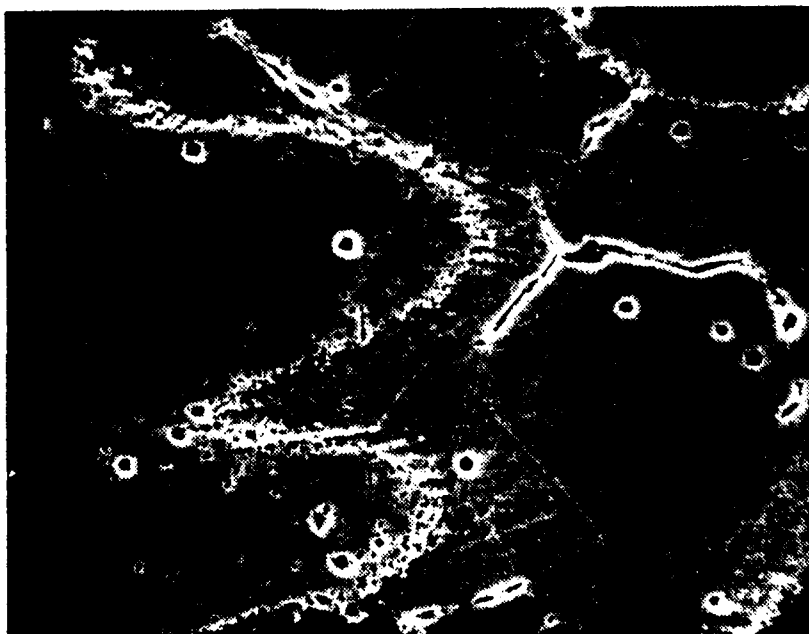Figure 52.   AISI 304, annealed, irradiated then etched, 1310X SEM.

Figure 53.   Same as above

84

Figure 54.   AISI 304 annealed, irradiated then etched, 400X optical.

Figure 55.   Same as above.

85

This result is interesting and a complete investigation needs to be conducted. However, the following preliminary facts may have a significant bearing on the solution:

(a) The metallic glass area is that area in which a sufficient amount of energy has been deposited to melt the surface. We should expect some residual heat left here when the arcing occurs. It's reasonable to suspect that less energy from the sheath potential is required to initiate arcing in this hotter area. This idea of thermionically assisted field emission is not new [11, 33] . If the plasma sees the same "type" of material we would expect more arcing on the hotter areas than on the cooler areas.

(b) The metal glass film is very thin with perfect bonding to the base metal. Perhaps the metallic glass layer is too thin to influence the arcing mechanism. This would allow arcing density more like the base metal than the metallic glass films studied earlier. (c) When we etch the base metal the arc crater rims are etched away leaving just the crater spot in its center. This crater spot is almost identical to the holes left by the etchant itself, see figures 58, 59 . It's possible to be confused in the base metal as to which craters are arc craters and which are due to the etchant. (d) The commercial metallic glass composition is significantly different than the AISI 304 metallic glass of the thin film on our targets and the
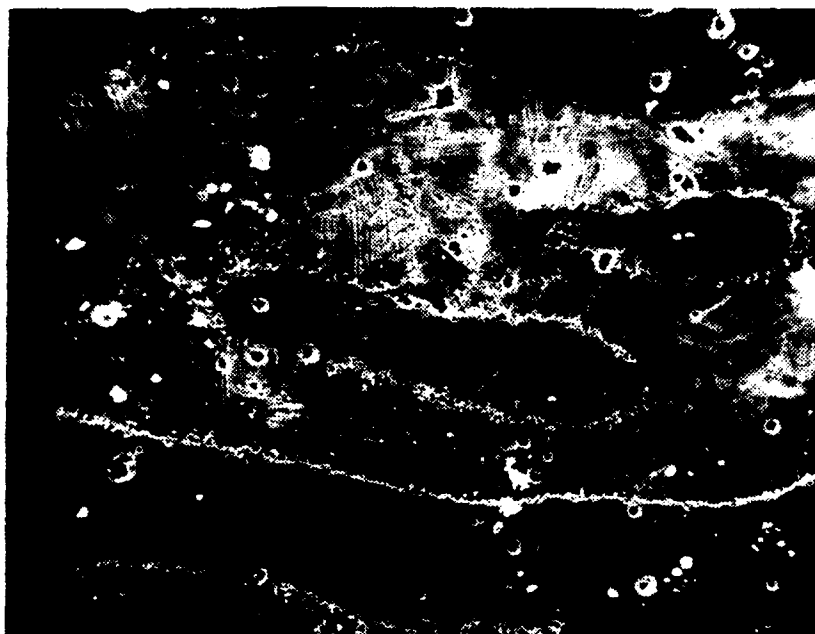
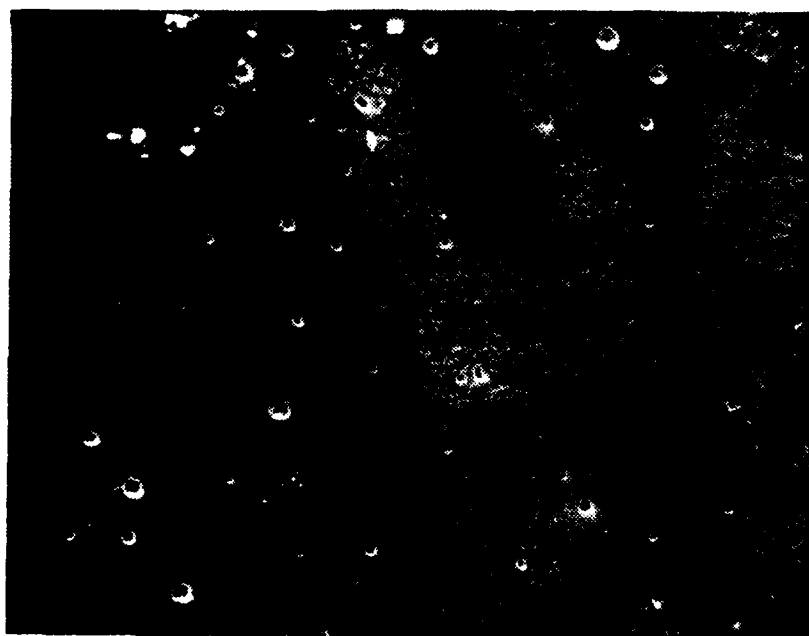Figure 56. AISI 304 stainless, irradiated then etched,
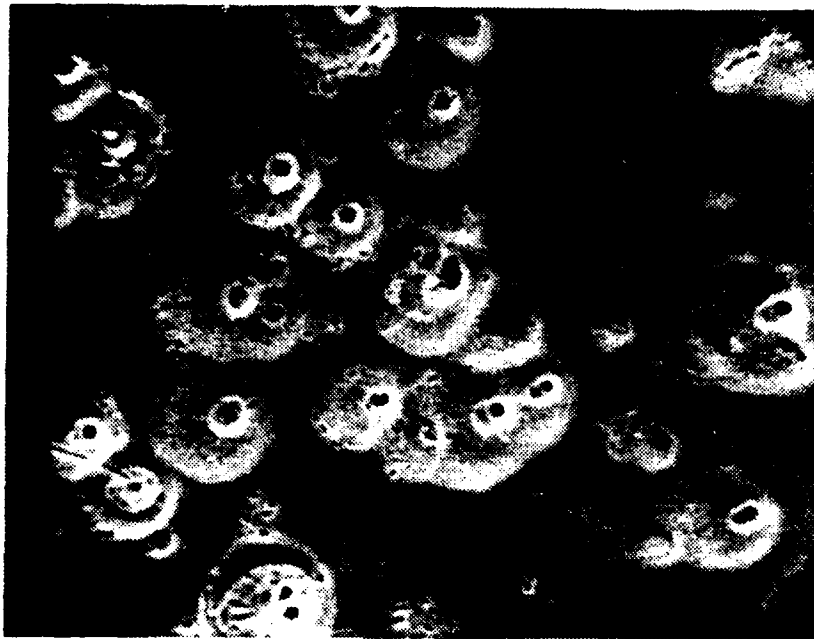SEM 650X.

Figure 57. Same as above.

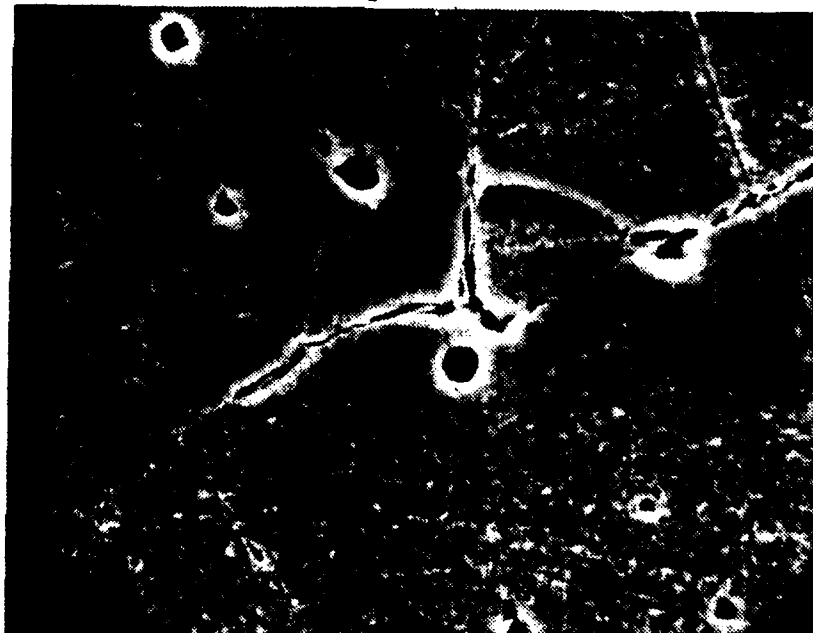Figure 58. AISI 304 annealed, irradiated then etched, 1310X, metallic glass area.

Figure 59. Same material as above, 2620X, far from unipolar arcing area.

Figure 60.   AISI 304 stainless, irradiated then etched.
SEM 6300X.

comparison with our earlier study of the commercial metallic glass may not be valid.

Another important observation can be made from figure 60. In the literature there have been two proposals for the formation of the crater rims. One proposal states that the metal is melted at the bottom of the arc crater and that the molten metal is pushed out of the crater by the high pressures which exist there. The metal then flows out of the crater and forms the crater rim. The other theory suggests that the arcing softens the metal surface and that the high pressures which exist immediately above the crater pushes this melted surface metal out into the characteristic crater rim shape. Because the cathode spot crater is so much deeper than the surface layer of metallic glass we should be able to differentiate which theory is correct. In the one case, the crater rims would be formed out of AISI 304 base metal, in the other case the crater rims would be formed out of the metallic glass. The metal surface shown in figures 58, 60 have been etched after the plasma surface interaction. If the crater rims were base metal they would have been etched away. The fact that they are still evident supports the second theory of crater rim formation, that is: that the high pressures which exist immediately above the cathode spot deform the melted surface into the characteristic crater rim formation.

In summary, we have produced metallic glass as a thin surface layer by melting and rapid quenching areas of the target surface. This rapid heating would have destroyed any microwhiskers on the order of 10^{-8}m, yet arcing occurs. The concept of microwhiskers is well established in the literature. However, the fact that they have never been seen though features of a few tens of nanometers could be detected, together with the results of the present experiment, clearly show that the concept of microwhiskers as arc initiation sites is not necessarily valid.

B. GRAIN BOUNDARIES

The inability to find microwhiskers on highly polished metal cathodes led several researchers to speculate that arc initiation occurs at sites of low work function such as grain boundaries and cracks [28, 34-35].

A group of investigators at Columbia [34] have completed experiments on unipolar arcing in a shock tube environment. They conclude that grain boundaries are definitely preferred sites for unipolar arcing. Two aspects of their work should be questioned. First: all samples were pre-etched. This provided the surface with sharp edged depressions at the grain boundaries. It is precisely this fact that the etchant selectively attacks the grain boundaries which is used to make them visible. We might expect these sharp edges to yield an enhanced electric field and thereby

increase the probability of arcing, arcing because of the new surface features and not because of the grain boundary work function. The second point is the fact that they used a hot deuterium plasma and reported that all of their targets were covered with deuterium pressurized blisters. It is well known that gases are absorbed preferentially at grain boundaries because of the vacancies and lattice imperfections which exist there. We should expect the blistering to occur first at those areas which more easily absorb the gas. The blistering occurs first at the grain boundaries and we should expect unipolar arcing at these blistering sites because the raised blisters yield an enhanced electric field, not because of the grain boundary work function.

To overcome the above problems a new experiment was devised. In a vacuum chamber a laser produced plasma generated unipolar arcing on the highly polished target surface. The plasma is self consistent, that is, it is made of the same material as the surface it is in contact with. This removes any possibility of blistering. Both targets etched after exposure to the plasma and those etched before exposure were used.

Targets of AISI 304 annealed, AISI 316 annealed, 1010 mild steel and pure aluminum were used. See figures 61-76. The stainless steels were annealed to increase the grain size so that the grain boundaries would be clearly

distinguishable. The annealing process called for annealing at 1950 F for one hour and then water quenching. The micrographs show areas relatively far from the main laser crater area. In areas where the plasma density and temperature are so low that unipolar arcing is just barely established. It is in these areas that we would expect grain boundaries to influence the arc initiation if they do anywhere. In all cases the arc density was a function of the distance from the laser impact area but otherwise the arcs were randomly distributed with no preference for the grain boundary location. Grain boundaries play no significant role in unipolar arcing.

C. PLASMA PERTURBATIONS

Fairly large surface defects and contaminants do contribute to field enhancement factors. These factors together with the Fowler-Nordheim model accurately predice emission currents. For clean polished cathodes, on the other hand, neither microwhiskers nor grain boundaries can cause the required field enhancement for onset of unipolar arcing on smooth surfaces. It would be difficult to propose any other surface characteristic which might satisfy this requirement. We are led, therefore, to propose a new concept: Field enhancement can be caused not only by surface inhomogeneities but also by inhomogeneities within the plasma. In support of this argument, see figures 77, 78 which clearly show
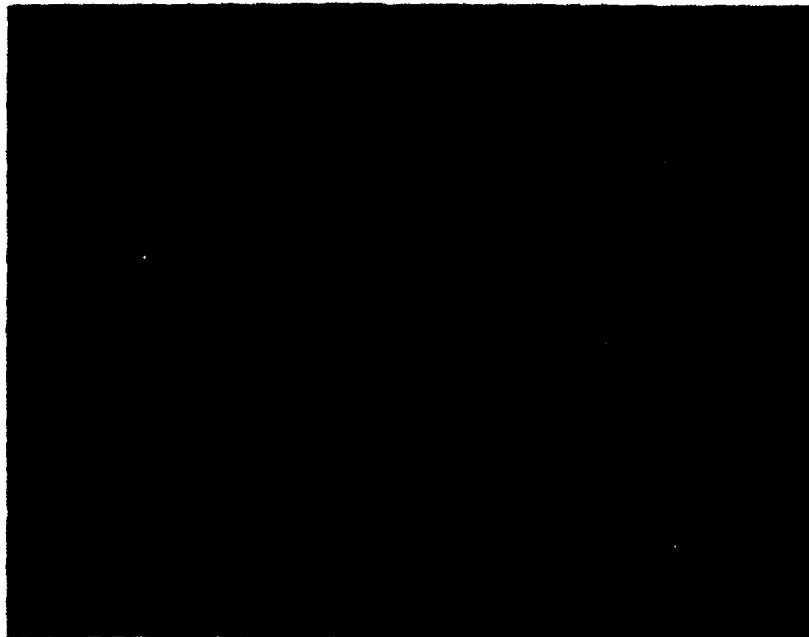
93

Figure 61. AISI 316 steel, etched before irradiated, optical 1000X.

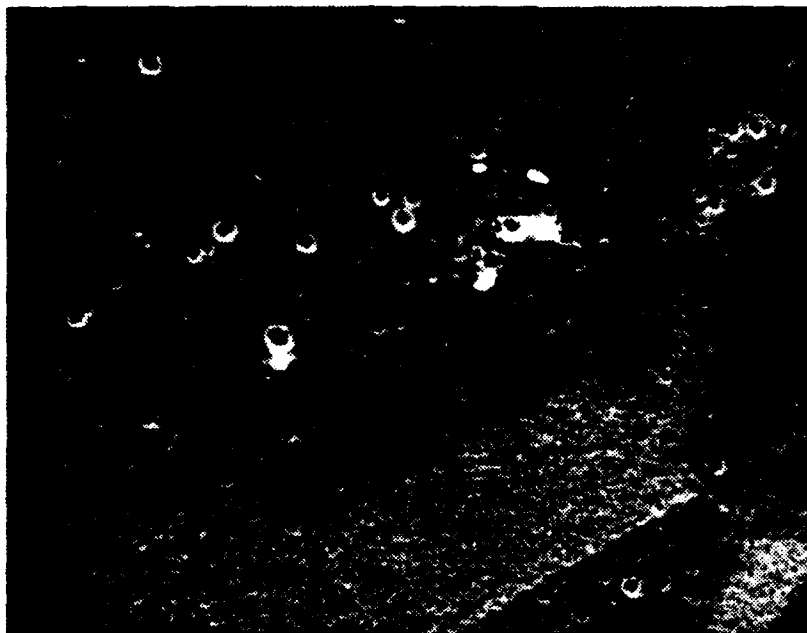Figure 62. AISI 316 steel, etched before irradiated, optical 1000X.

94

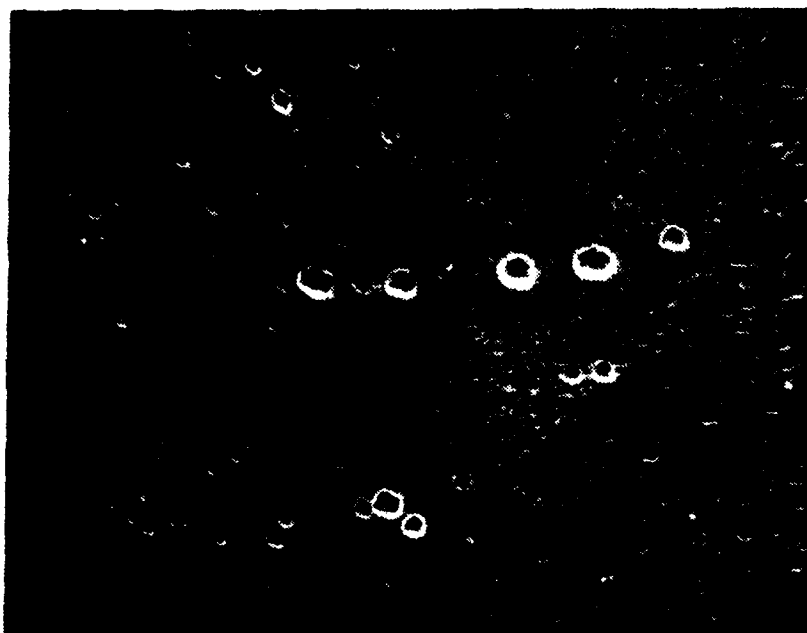Figure 63. AISI 316 stainless, irradiated then etched, SEM 1000X.

Figure 64. Same as above.
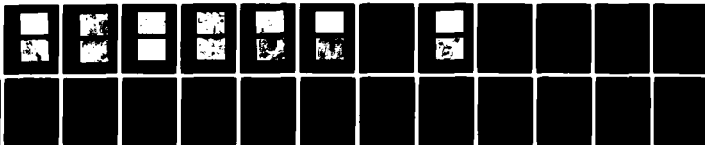
Figure 65. Pure aluminum, etched after irradiated, optical 1000X.
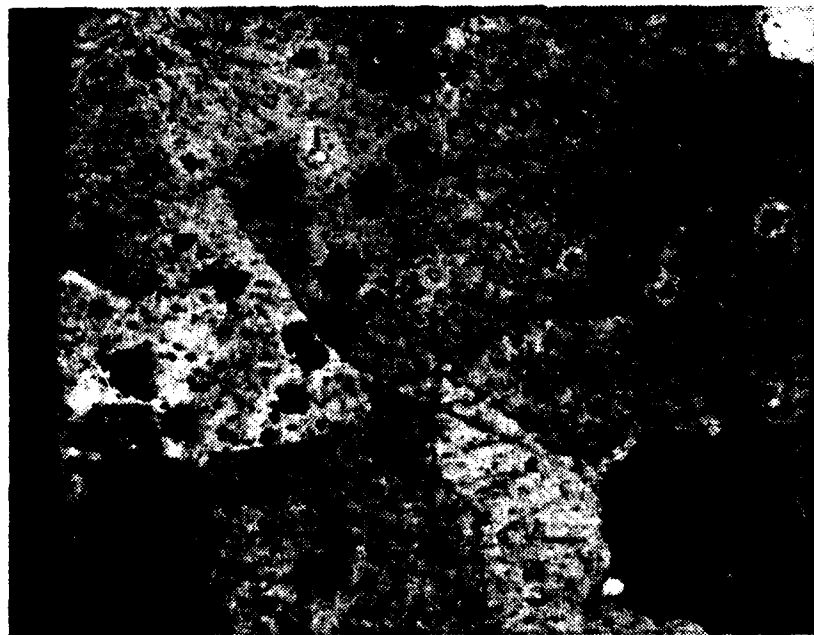
Figure 66. Pure aluminum, etched after irradiated, optical 400X.

96
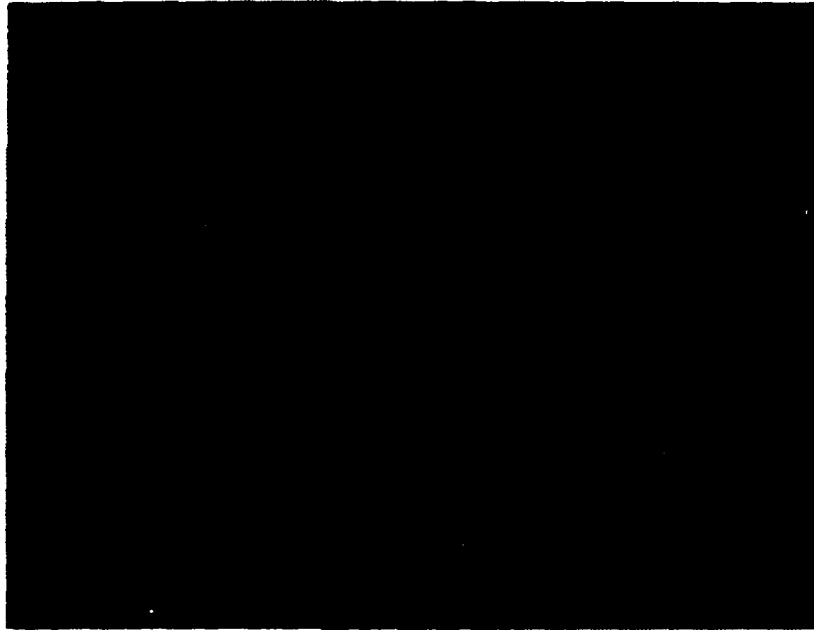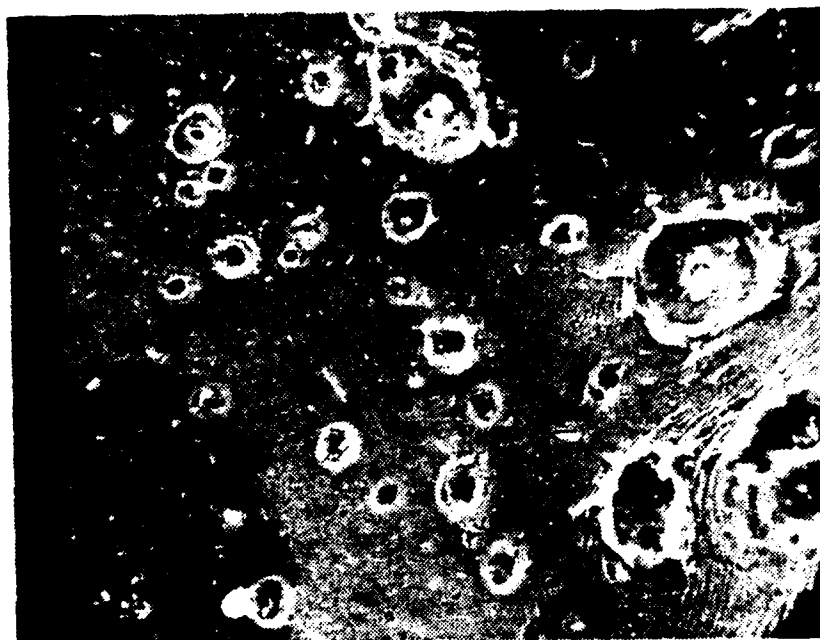
Figure 67. Pure aluminum, etched after irradiated, SEM 650X.
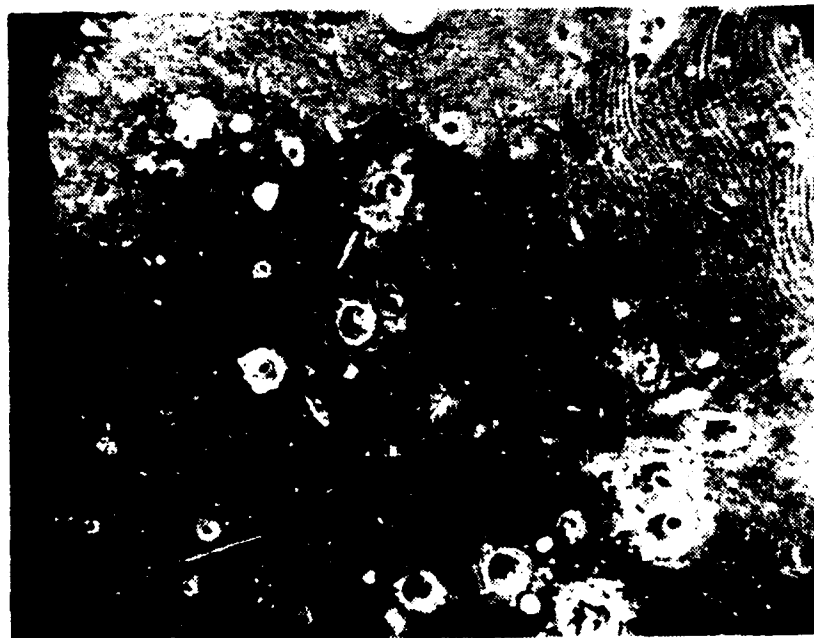
Figure 68. Pure aluminum, etched after irradiated, SEM 650X.

97
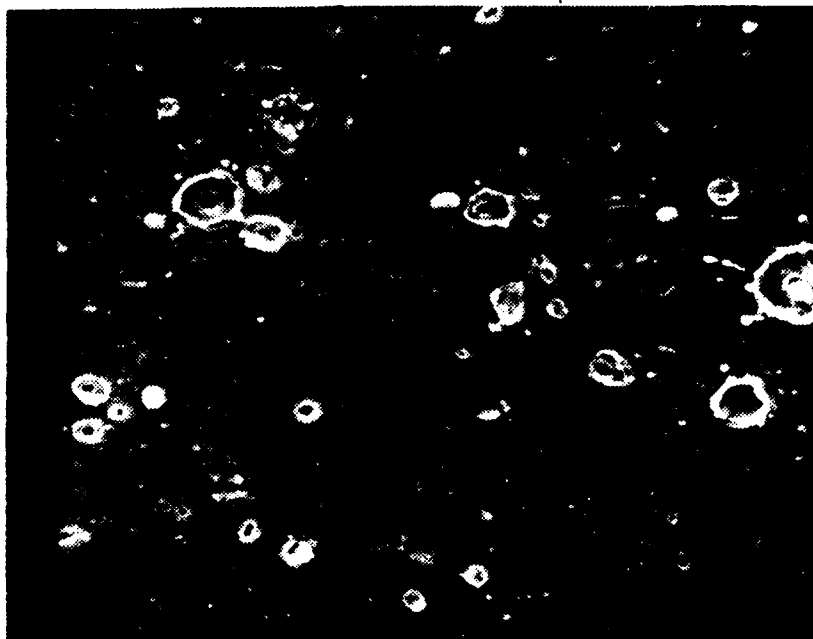
Figure 69. Pure aluminum, etched before irradiated,
SEM 540X.

Figure 70. Pure aluminum, etched before irradiated,
optical 400X.

Figure 71. 1010 mild steel, etched, not exposed
to the plasma, 1050X.

Figure 72. 1010 mild steel, etched after irradiated,
1100X.
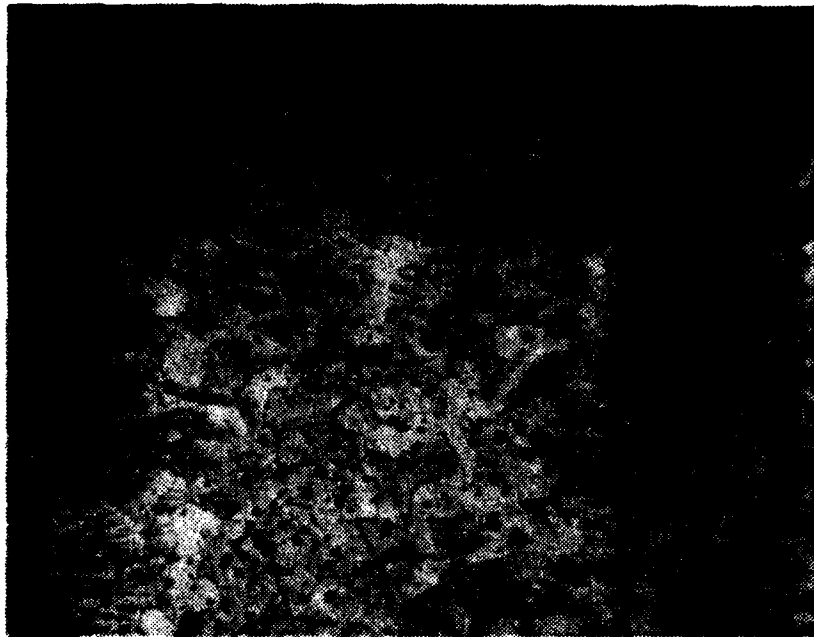
Figure 73. 1010 steel, etched after irradiated,
optical 200X.
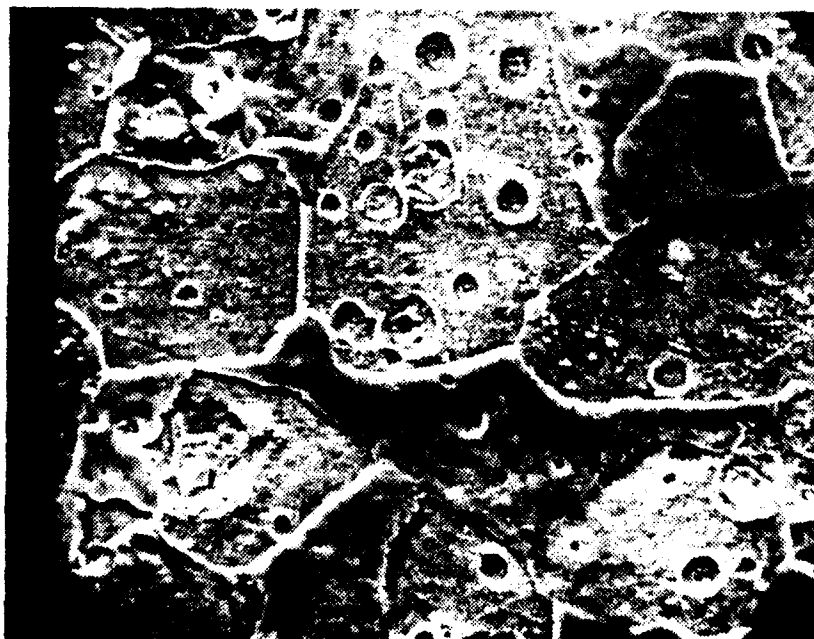
Figure 74. 1010 steel, etched after irradiated,
SEM 1100X.

100

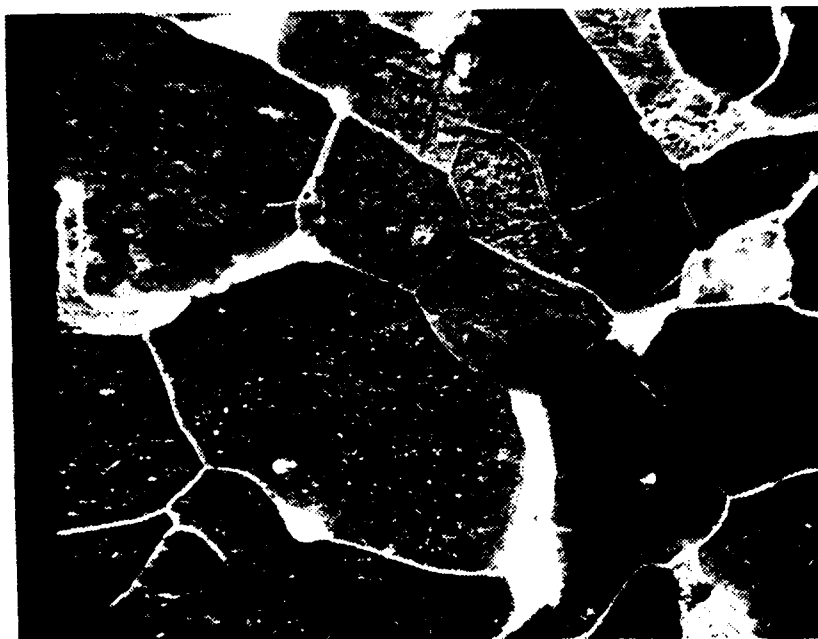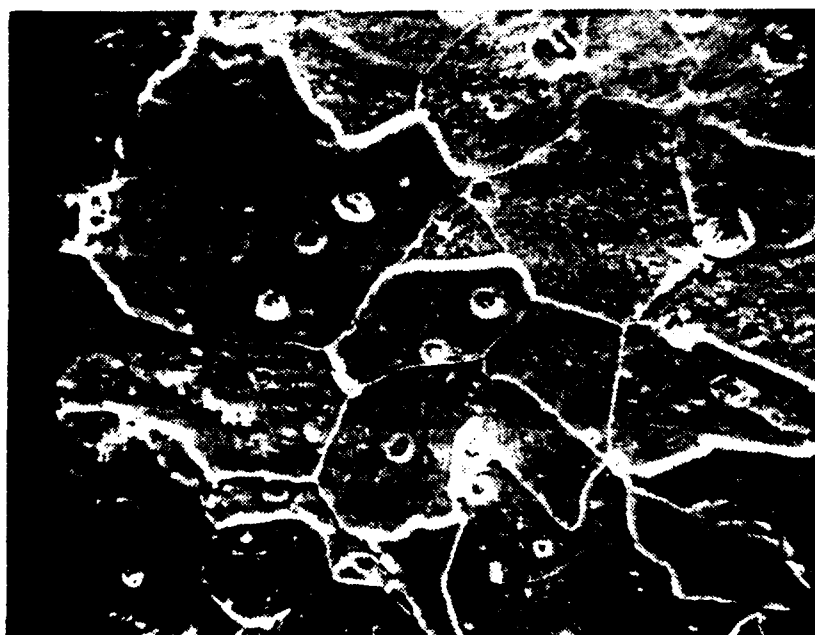Figure 75.   1010 steel, etched before irradiated,
             SEM 1300X.
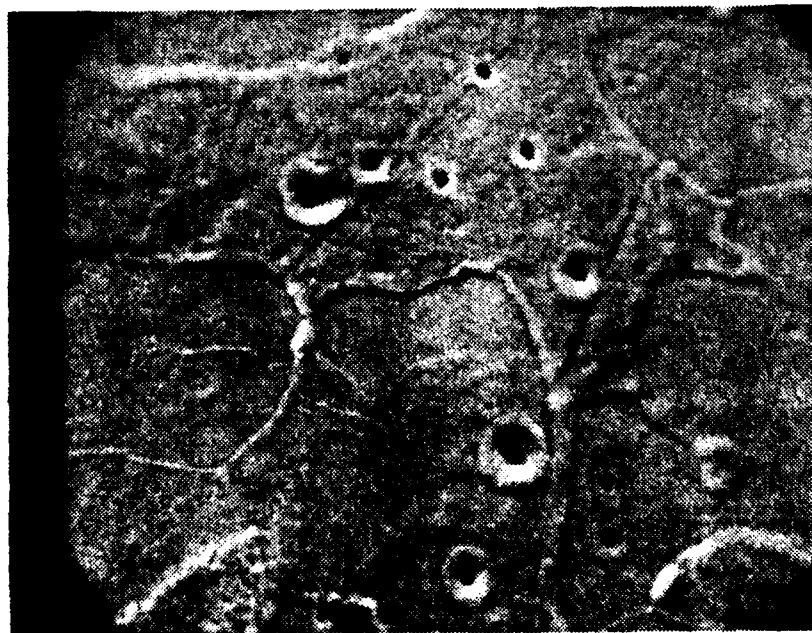
Figure 76.   1010 steel, etched before irradiated,
             SEM 1350X.

cases in which two adjacent arcs burn at the same time,
thereby forming a single crater rim with more than one
cathode spot. The fact that adjacent arcs can burn simul-
taneously on the metal surface would require that these arcs
are also simultaneously sustained within the plasma. It
would seem that this could only occur if the adjacent areas
within the plasma were separated by some small area of lower
electric potential, if not, only one arc would have burned.
This, of course, is only possible if there are electric
field perturbations in the plasma. A plasma pressure gradi-
ent generates an electric field component in the opposite
direction to the gradient. A local density gradient in the
plasma generates a locally enhanced field due to the
pressure gradient and a thinner plasma sheath due to the
higher plasma density, both of which enhance the local field.
In other words, there are variations in the plasma sheath
thickness. This thickness is given by the Debye length
which is inversely proportional to the square root of the
density. A local increase in plasma density could determine
the individual arc initiation site.
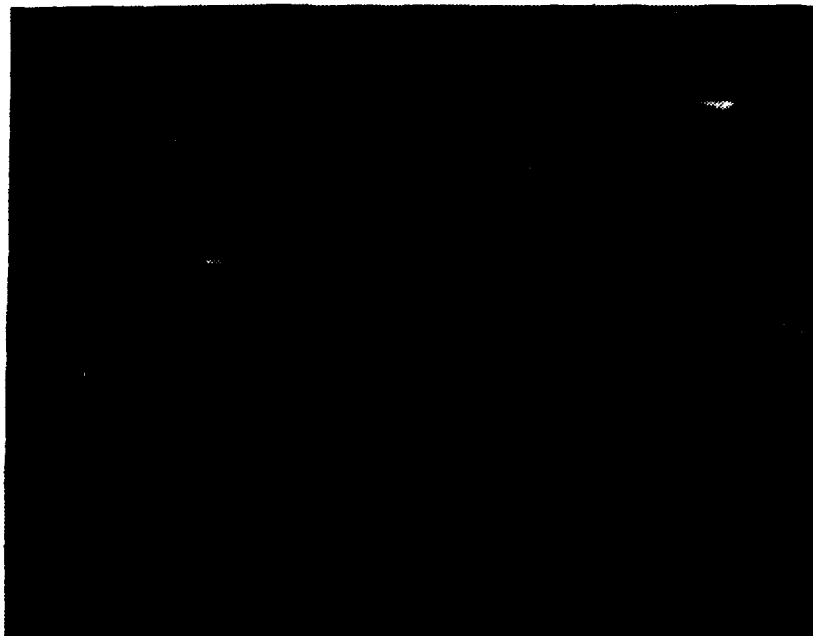
Figure 77.   AISI 304, showing double and triple cathode spots
within a single crater, 1000X.
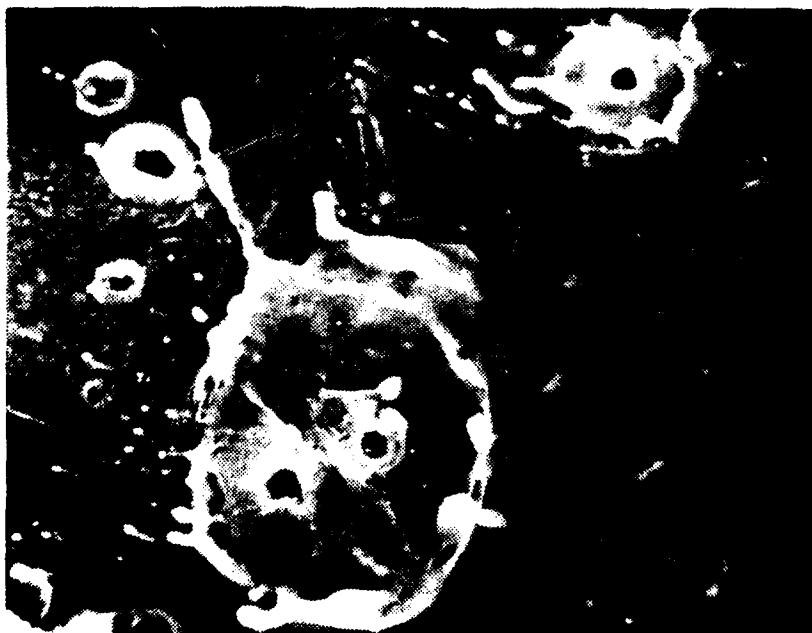
Figure 78.   Pure aluminum, showing two cathode spots in a
single crater, 1300X.

103

VI. ARC MOTION

The retrograde motion of the cathode spot in a magnetic field remains one of the most intriguing riddles of arc physics. When a transverse magnetic field acts on a direct current cold cathode arc the positive column is always deflected in the same direction as would be a solid conductor. Under certain pressure and field conditions the cathode spot moves in the opposite (retrograde) direction, dragging the deflected column with it. The arc as a whole moves contrary to Ampere's rule. The effect was first observed in the low pressure mercury arc [37] , and later confirmed by many researchers [24, 38-58] . This phenomenon has been found in many metals (Cu, Ag, Zn, Mg, Al, Pb, Fe, Ni, Co, Mn, and W) and in various gases (Ar, N_2, O_2, CO_2) [8, 19, 23, 24, 26, 28-37, 42, 50, 54, 55, 57-64] . In all cases the motion is in the retrograde direction if the pressure is sufficiently low. This critical pressure is itself a function of arc current and applied magnetic field. The critical pressure is proportional to the magnetic field and inversely proportional to the arc current. The velocity of the retrograde arc, on the order of 10^2cm/sec, rises with rising current and also with increasing magnetic field. These critical pressures for velocity reversal ranged from 1-60 Torr [88] . Several experimenters have noticed an abrupt doubling of the retrograde velocity for pressures between 1 Torr and 2 Torr

[43, 55, 65-67] . The arc motion is also affected by a separation of the electrodes. The critical reversing pressure increases with decreasing separation [59, 60] and very short arcs (0.5mm) have been driven in the retrograde direction in atmospheric air [53] . There have been several reports of immobility observed in short arcs which over a range of conditions cannot be driven in either direction [54, 61, 68] but a new study shows that arcs in transverse magnetic fields move at various velocities but no absolute immobility occurs. Velocities down to 3m/sec were recorded [69] . The same report demonstrates a strong dependence of velocity on oxide film thickness and surface roughness.

There has been a myriad of theories to explain these effects [25, 58, 67, 70-74] . Of these suggestions none are qualitatively consistent with all of the observations and many are inconsistent with known conditions near the cathode spot.

There are three present day theories which deserve a closer look:

      (a)   The Robson and Von Engel Model [42, 74] .

      (b)   The auweter-Ming, Schrade Model [75] .

      (c)   The successive Explosion Model [25-27, 46] .

In the Robson, Von Engel theory the arc column is observed to be deflected in the Amperian direction and to be strongly curved in the vicinity of the cathode spot [42] .

It was suggested by Robson and Von Engel [41] that the magnetic field acting on the arc near the cathode spot is the resultant of the applied field H_o and the self field i/R, where i is the arc current and R is an effective radius of curvature of the arc column where it joins the spot (figure 79). The direction of motion is then determined by the direction of the resultant field H, given by $H = H_o - i/R$. Retrograde motion occurs if the self field exceeds the applied field.

Smith [76] describes the Robson, Von Engel arc model by dividing it into three regions near the cathode spot (figure 80). α is a long horizontal round section, β the elbow, γ is the remainder, including the current in the massive cathode. The induced field due to a semi-infinite bar of radius a (region α) at the point K is $H_\alpha = i/10a$. The field due to region γ is also $H_\gamma = 1/10a$ and the field due to the 90 degree elbow is $H_\beta = 2 i/15a$. Adding the fields of α, β and γ we have $H(\text{induced}) = i/3a$ out of the paper. We must now find the direction of the resultant force on the arc column. Let Q be the force per unit area directed in the retrograde sense. Let A be the force per unit area in the proper or Amperian direction.

$$Q = \frac{(H - H_o)^2}{8\pi} \text{ dynes/cm}^2 , \quad A = \frac{(G + H_o)^2}{8\pi} \text{ dynes/cm}^2$$

G is the field due to the arc current on the convex side of the arc path. Its value is less than H and is in the same

106
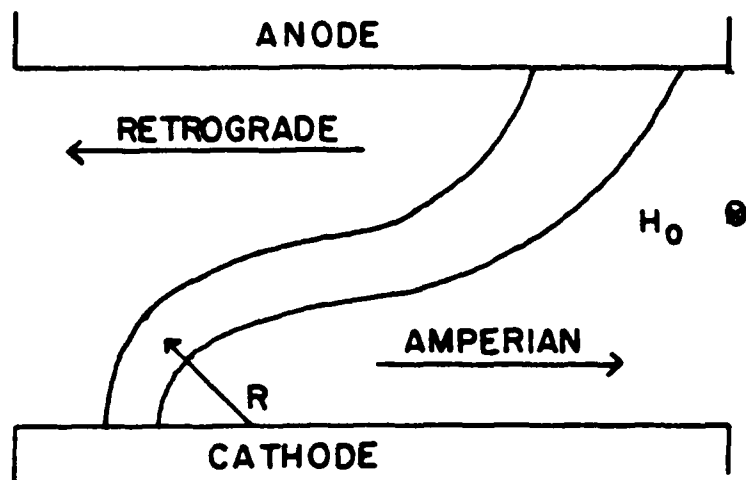
Figure 79.   The shape of an arc in a transverse magnetic field.
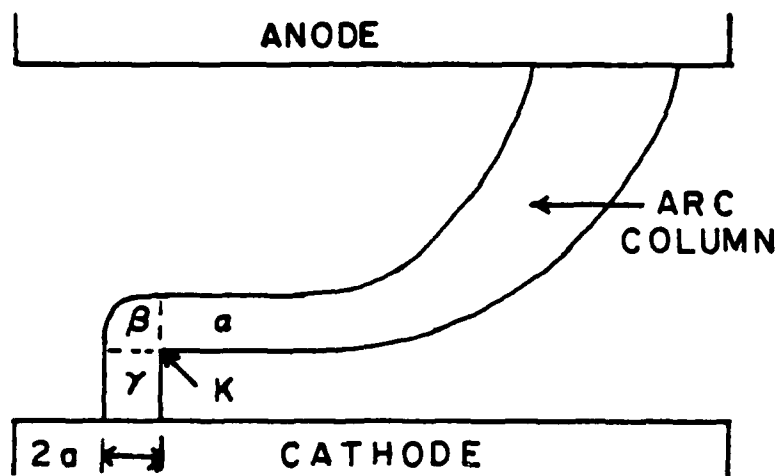
Figure 80.   Approximate shape of an arc in a transverse
magnetic field.

sense as H_o . To yield a resultant force per unit area in the retrograde direction, $H - H_o$ must be greater than $G + H_o$, hence $H > 2H_o$. The comparison of Q and A seems a fair one since a more rigorous treatment leads to a relative increase of A over Q . In the Smith experiments, $2H_o$ ranged upward to values near 10,000 oersteds. Also, H appears to be greater than could really exist, since to get it a relatively high current density was chosen and also the radius of the positive column at the bend and in region α was taken to be 0.001 cm, whereas expansion of the arc path as it leaves the cathode is expected to make the radius larger than that. It seems that the resultant force is preponderantly in the Amperian direction and the Robson, Von Engel theory is not sustained. Twenty years later Robson [74] counters Smith's objections with two observations which he feels support the original theory. The first is the sideways drift of an arc when there is a component of the field normal to the cathode. This is evidence for the exist-ence of currents flowing parallel to the cathode and suffi-ciently close to the spot to affect its motion [78] . As we've just seen the Smith treatment included just such a current in region α and we can not accept this as grounds for ruling out the Smith objections. Robson's second point is the fact that retrograde motion is not found in thermionic arcs where the current density at the cathode is several orders of magnitude less than in the cold cathode arc, and

the size of the spot is correspondingly greater. This is also a poor argument. Smith's whole point was that for all of the conditions found, whether in a cold cathode arc or in a thermionic arc, the Robson, Von Engel model leads to the Amperian motion and retrograde motion can not be achieved with this model.

The second model we should look at is the Auweter-Ming, Schrade model [75]. This model requires a nonsymmetric current distribution within the arc channel. This would lead to nonsymmetric arc craters and nonsymmetric pressure distribution due to evaporated metal neutrals about the arc crater. The authors assume a Maxwellian distribution of the evaporated metal above the gaseous half space of the cathode arc. The theory leads to the conclusion that the channel bends preferably in the retrograde direction, i.e. opposite to the $J \times B$ direction. As a consequence of the instability, the discharge channel may bend so far that it touches the cathode surface at another place thereby heating the metal surface and eventually creating another current carrying spot. In the case of no external magnetic field the new spot has no preferred direction and therefore jumps statistically, while within a transverse magnetic field the spots jump preferably in the retrograde direction provided the current density maximum is shifted in the retrograde direction. The net force on the arc channel causes a turn of the bent channel into the retrograde direction as long

as the channel diverges. If the channel converges the bent channel should turn in the JxB direction. Since we must expect that for a converging channel (converging in the current direction) the vapor pressure is larger and the electric current density smaller than they are for a diverging channel, we may conclude with respect to the stability criteria that the cathode spot jumps more likely in the retrograde direction than in the Amperian direction. Unfortunately the arc column has been observed under various conditions for both Amperian and retrograde arcs. The arc channel always converges in the current direction and is swept back from the cathode spot in the Amperian direction for either retrograde or Amperian motion [38, 44]. This model fails to incorporate the facts.

The final model which still has its followers is the Successive Explosion model [24-27]. The central features of the explosion model include the following concepts: The cathode spot is formed when a microwhisker produces fields high enough to cause electron field emission with current densities sufficiently high flowing through the tip of the microwhisker so that resistive heating causes a very rapid explosion like evaporation of this microwhisker. The explosion debris is a plasma which spreads along the cathode surface, increasing the conductivity near the next microwhisker on the cathode surface and causes field emission current through that microwhisker tip. However, due to the

sharp drop of voltage after the plasma channel has formed no
explosion of this microwhisker occurs but just the current
continuity is established. As the plasma produced during
the explosion flies out and cools its conductivity decreases,
the voltage drop increases until explosive breakdown occurs
at another suitable microwhisker and the cycle repeats. Thus
the neutral vapor necessary for regeneration of the near
electrode plasma is produced as a result of microwhisker
explosion, or of several neighboring microwhiskers, at the
moment of spot initiation. The current for the total life-
time of the spot is achieved by field emission from the
microwhisker site with current densities much smaller than
that for the original microwhisker. This model purports to
explain retrograde arc motion by the following argument:
During the explosion process the ions move from the cathode
into the discharge gap and the region of maximum concentra-
tion of ions is displaced in the retrograde direction.
Within this model the inversion of forward motion with
increasing pressure can be understood from the fact that
the breakdown displacement of the ions during the time of
forming the conductive channel is sharply reduced by the
residual gas so that the back displacement turns out to be
smaller than the size of the spot. The explosion model of
course relies on the assumption that microwhiskers are
required for arc initiation. In the previous section on
arc initiation, considerable evidence was found that

111

microwhiskers are not a requirement for unipolar arcing on smooth surfaces. Without microwhiskers this theory fails.

In conclusion it is clear that there has not been to date a satisfactory explanation for retrograde arc track motion. In spite of the seventy-five years of investigation, [37] , no theory has yet explained all of the facts associated with this phenomenon. The investigation has been complicated by the small size scale, short time scale and the difficulty of establishing controlled and reproducable experimental conditions.

VII. CONCLUSION

The work on this thesis has been wide in scope. An
attempt to join a number of diverse experimental facts and
widely varying theories into a single consistent theory of
unipolar arcing is admittedly ambitious. Hopefully, however,
others will take this lead and work toward a single adequate
theory of unipolar arc initiation, cessation, and motion,
consistent with the observed facts. It is our belief that
this new theory will be formulated in terms of plasma
physics and that the preliminary theoretical groundwork
needed to develop such a theory is in hand.

Toward this end several important conclusions have been
made within this thesis:

Commercially produced solid metallic glasses show a much
higher unipolar arc resistance than the metals from which
they are made. Laser heating of metal surfaces can form
thin metallic glass films. More research is needed, but it
would seem reasonable that adequate metallic glass layers
can be produced on metal components used in a plasma environ-
ment. This would provide all of the good structural proper-
ties of the steel without any of the adverse mechanical
properties and higher costs associated with coatings to
reduce unipolar arcing.

Nickel is susceptible to unipolar arcing. It was
reported previously to be quite arc resistant but the resear-
chers failed to account for the arc craters disguised by the
flowing molten metal.

113

On the topic of arc initiation sites on highly polished metal surfaces, the long standing concept of the requirement of microwhiskers for unipolar arc initiation is no longer valid. The alternative proposal that grain boundaries act as preferred initiation sites is also not valid. There is some evidence that electric field enhancement can occur in the plasma sheath itself due to local density gradients. Consequently there is a limit to the improvement that can be achieved by surface cleaning and polishing.

New evidence was found which supports the idea that crater rims are formed by the high pressure plasma generated above the cathode spot as part of the arcing process.

Finally, the way arcs move, whether vacuum arcs or unipolar arcs, remains a mystery. There has been to date no adequate theory of arc motion.

VIII. RECOMMENDATIONS

The results of this thesis lead to several related important areas of study. The Naval Postgraduate School Plasma Laboratory offers an excellent facility for studying the effects of laser induced plasma-surface interactions over a large range of pressures and different atmospheres. The current program of evaluating different candidate Tokamak wall and limiter materials for unipolar arc resistance should be continued.

This thesis showed that the exposure of the target material to a single laser pulse caused a rapid melting and quenching which changed the molecular structure of the target surface material from a crystalline metal to an amorphous metallic glass in the laser impact crater area. It is recommended that experiments be carried out to determine if a smooth metallic glass coating can be formed on the base target material by defocussing the laser so that enough energy is deposited to form the glass without producing a hot plasma that arcs the surface. The laser-produced metallic glass coating could then be exposed to a hot dense plasma to evaluate its resistance to unipolar arc damage. If carried out, these experiments might explain the apparently contradictory results obtained in this thesis between commercially prepared metallic glass alloys which showed little or no unipolar arcing and the laser-produced metallic

glasses surrounding the impact crater which showed heavy arcing.

Further experiments on different commercially prepared metallic glass alloys would appear worthwhile. The glasses evaluated in this thesis not only demonstrated a very high unipolar arc resistance and less laser-surface interaction damage than their parent crystalline structures, they have excellent engineering qualities such as toughness, ductility, and corrosion resistance.

The availability of a new high speed (1 nanosec/div) oscilloscope in the plasma laboratory would make it possible to obtain much better plasma characteristic measurements than in previous studies. It would be worthwhile to measure the laser-induced plasma parameters such as density and temperature on this very fast timescale at different spatial positions. The availability of this data would then make it possible to correlate plasma parameters with observed unipolar arc crater locations and densities. Also, this could provide the data needed to establish the validity of the proposed current unipolar arc models.

LIST OF REFERENCES

1. McCracken, G. M., and Stott, P. E., "Plasma-Surface Interactions in Tokamaks." _Nuclear Fusion_. To be published. Culham Laboratory Preprint, 1979.

2. Tazima, T., "First Wall Design Considerations of JT-60 and Related Experiments," _Journal of Nuclear Materials_, 76 & 77, p. 594-599, 1978.

3. Behrisch, R., "Surface Erosion From Plasma Materials Interaction." _Journal of Nuclear Materials_ 85 & 86, p. 1047-1061, 1979.

4. McCracken, G. M., and Goodall, D. H. J., "The Role of Arcing in Producing Metal Impurities in Tokamaks." Nuclear Fusion. To be published. Culham Laboratory Preprint, 1977.

5. Goodall, D. H. J., Conlon, T. W., Sofield, C., and McCracken, G. M., "Investigations of Arcing in the DITE Tokamak." _Journal of Nuclear Materials_ 76 & 77, p. 492-498, 1978.

6. McCracken, G. M., and Stott, P. E., "Plasma-Surface Interactions in Tokamaks." Culham Laboratory (HEAP) Report CLM, p. 573, 1979.

7. Schwirzke, F., and Taylor, R. J., "Surface Damage by Sheath Effects and Unipolar Arcs." _Journal of Nuclear Materials_ 94 & 95, 1980.

8. Chen, F., _Introduction to Plasma Physics_, Plenum Press, New York, N. Y., 1974.

9. Robson, A. E., and Thonemann, P. C., "An Arc Maintained on an Isolated Metal Plate Exposed to a Plasma." _Institution of Electrical Engineering_, V. 106, Pt. A, Supp. 2, April 1959.

10. Miley, G. H., "Surface Effects Related to Voltage Breakdown in CTR Devices." _Journal of Nuclear Materials_, 63, p. 331-336, 1976.

11. Daalder, J. E., "A Cathode Spot Model and its Energy Balance for Metal Vapour Arcs." _Journal Physics, D._, Vol. 11, 1978.

12. Hantzsche, E., Juttner, B., Puchkarov, V. G., Rohrbeck, W., Wolff, H., "Erosion of Metal Cathodes by Arcs and Breakdowns in Vacuum," _Journal of Physics D: Applied Physics_, Vol. 9, 1976.

13. Smithells, C. J., _Metals Reference Book_, Fifth Edition, Butterworths, London & Boston, 1976.

14. Guile, A. E., and Juttner, B., "Basic Erosion Processes of Oxidized and Clean Metal Cathodes by Electric Arcs." _IEEE Transactions on Plasma Science_, Vol. PS-8, No. 3, September 1980.

15. Union Carbide Electronics, _KORAD Laser Systems Instruction Manual for Nd: Glass Laser_, five volumes, KORAD Department, Santa Monica, California, 1969.

16. Davis, L. J., _Self-Generated Magnetic Fields Produced by Laser Bombardment of a Solid Target_, p. 14-30. M.S. Thesis, U. S. Naval Postgraduate School, Monterey, California, 1971.

17. _Metals Handbook_, 8th Edition, Vol. 2, American Society for Metals, 1964.

18. Barker, H. J., and Rush, R. J., _An Investigation of Plasma-Surface Interactions on Selected Conductors and Insulators_, M.S. Thesis, U. S. Naval Postgraduate School, Monterey, California, 1980.

19. Chaudhari, P., Giessen, B. C., Turnbull, D., "Metallic Glasses," _Scientific American_, April 1980.

20. Gillman, J., "Ferrous Metallic Glasses," _Metal Progress_, July 1979.

21. Taylor, D., "How a Laser Glazer Makes Alloys Go Glassy," _New Scientist_, 17 March 1977.

22. Cobine, J. D., _Gaseous Conductors Theory and Engineering Application_, p. 116-119, McGraw Hill, 1941.

23. Boyle, W., Kisliuk, P., and Germer, L., "Electrical Breakdown in High Vacuum," _Journal of Applied Physics_, v. 26, p. 720-725, June 1955.

24. Il'in, V., and Lebedev, S., "Destruction of Electrodes by Electric Discharges of High Current Density," Soviet Physics-Technical Physics, v. 7, No. 8, p. 717-721, 1963.

25. Fursei, G. N., and Vorontsov-Vel'yaminov, P. N., "Qualitative Model of Initiation of a Vacuum Arc II, Field Emission Mechanism of Vacuum Arc Onset." Zhurnal Teknicheskoi Fiziki, v. 37, p. 1870, 1967. (Soviet Physics; Technical Physics, v. 12, p. 1370, 1968.)

26. Mesiats, G. A., Proceedings of the Tenth International Conference on Phenomena in Ionized Gases, Oxford, 1971.

27. Rakhovskii, V. I., "Experimental Study of the Dynamics of Cathode Spots Development," IEEE Transactions on Plasma Science, v. PS-4, No. 2, p. 81-102, June 1976.

28. Cox, B. M., "The Nature of Field Emission Sites," Journal of Physics D: Applied Physics, v.8, p. 2065-2073, 1975.

29. Vibrans, G. E., "Vacuum Voltage Breakdown as a Thermal Instability of the Emitting Protrusion," Journal of Applied Physics, v. 35, No. 10, p. 2855-2857, October 1964.

30. Latham, R. V., and Braun, E., Proceedings of the Third Symposium on Discharges and Electrical Insulation in Vacuum, Paris, (Paris: Imprimerie Louis-Jean), p. 123-127, 1968.

31. Breinan, E. M., Kear, B. H., and Banas, C. M., "Processing Materials with Lasers," Physics Today, v. 11, p. 44-50, November 1976.

32. Panofsky, W. K., and Phillips, M., Classical Electricity and Magnetism, p. 200-201, Addison Wesley, 1962.

33. Fabiniak, T. J., Jedynak, L., and Dodd, R. A., "Properties of Vacuum-Insulated Single-Crystal Tungsten Electrodes in High Electric Fields. Part II. Nature of Prebreakdown Currents," Journal of Applied Physics, v. 42, No. 6, p. 2240-2246, 1971.

34. Tien, J. K., and others, "Unipolar Arc Damage of Materials in a Hot, Dense Deuterium Plasma." Journal of Nuclear Materials, v. 76-77, p. 481-488, 1978.

35. Panayotou, N. F., and Tien, J. K., "Damage of a Candidate CTR Material in a High Energy Fluence Deuterium Plasma." Journal of Nuclear Materials, v. 63, p. 137-150, 1976.

36. Stark, V. J., "Induktienserscheimungen am Queeksilber-lichtbagen im Magnetfeld." Physikalische Zeitsehrift, v. 4, p. 440-443, 1902-1903.

37. Weintraub, E., "Investigation of the Arc in Metallic Vapours in an Exhausted Space." London, Edinburgh and Dublin Philosophical Magazine and Journal of Science, v. 7, p. 95-124, 1904.

38. Smith, C. G., "The Mercury Arc Cathode," Physical Review, v. 62, p. 48-54, July 1942.

39. Smith, C. G., "Cathode Dark Space and Negative Glow of a Mercury Arc." Physical Review, v. 69, p. 96-100, February 1946.

40. Gallagher, C. J., "The Retrograde Motion of the Arc Cathode Spot." Journal of Applied Physics, v. 21, p. 768-771, August 1950.

41. Robson, A. E., and Von Engel, A., "Origin of Retrograde Motion of Arc Cathode Spots." Physical Review, v. 93, p. 1121-1122, 1954.

42. St. John, R. M., and Winans, J. G., "Retrograde Motion of Cathode Spot in Transverse Magnetic Fields." Physical Review, v. 93, p. 653, 1954.

43. St. John, R. M., and Winans, J. G., "Motion of Arc Cathode Spot in a Magnetic Field." Physical Review, v. 94, p. 1097-1102, June 1954.

44. Grakov, V., and Hermoch, V., "Formation of Cathode Spots on Electrodes of Short-time High-Intensity Electric Discharge." Czechoslovak Journal of Physics, v. 13, p. 509, 1963.

45. Froome, K. D., "The Behaviour of the Cathode Spot on an Undisturbed Liquid Surface of Low Work Function," Proceedings of the Physical Society of London, v. 63. p. 377-385, 1950.

46. Kesaev, I. G., Cathode Processes in the Mercury Arc and Questions of its Stability, Gosenergoizdat Press, Moscow, 1961; Cathode Processes in the Mercury Arc, Consultants Bureau, New York, 1964.

47. Avramenko, V. B., and others, Thesis Reports on the XIV All-Union Conference on Emission Electronics, Tashkent, p. 23, 1970.

48. Rakhovskii, V. I., Proceedings of the Fifth International Symposium on Electrical Discharges and Insulation in Vacuum, Poznan, Poland, p. 215, 1972.

49. Rothstein, J., "On the Mechanism of Electron Emission at the Cathode Spot of an Arc," Physical Review, v. 73, No. 10, p. 1214, 1948.

50. Ecker, G., "Die Ercheinung des beweglichen Einfachund Mehrfachbrennflecks an der Kathode des elektrischen Lichtbogens," Zeitschrift für Physik, v. 136, p. 556-572, 1954.

51. Malter, L., "Anomalous Secondary Electron Emission A New Phenomenon," Physical Review, v. 49, p. 478, 1936.

52. Kantsel, V. V., Experimental Study of Cathode Spots with High Time Resolution, Ph.D. Thesis, Moscow, 1973.

53. Yamamura, S., "Immobility Phenomena and Reverse Driving Phenomena of the Electric Arc," Journal of Applied Physics, v. 21, p. 193-196, March 1950.

54. Zei, D., and Winans, J. G., "Motion of High Speed Arc Spots in Magnetic Fields," Journal of Applied Physics, v. 30, p. 1813-1819, November, 1959.

55. Smith, C. G., "Arc Motion Reversal in Transverse Magnetic Field by Heating Cathode," Physical Review, v. 73, p. 543, 1948.

56. Gallagher, C. J., and Cobine, J. D., "Retrograde Motion of an Arc Cathode Spot in a Magnetic Field," Physical Review, v. 71, p. 481, 1947.

57. Somerville, J. M., Electric Arc, in Russian, Gosenergoizdat Press, Moscow, 1952.

58. Smith, C. G., "Motion of the Copper Arc in Transverse Magnetic Field," Physical Review, v. 63, p. 217, 1943.

59. Smith, C. G., "Erratum: The Mercury Arc Cathode," Physical Review, v. 64, p. 40, 1943.

60. Smith, C. G., "A New Cold Cathode Arc," Physical Review, v. 83, p. 194, 1951.

61. Roman, W. C., Proceedings of the Sixth International Conference on Ionization Phenomena in Gases, Paris, v. 2, p. 287, 1963.

62. Weichel, H., Proceedings of the Seventh International Conference on Ionization Phenomena in Gases, Belgrade, v. 1, (Belgrade: Boris Kidvic Institute of Nuclear Sciences), p. 749, 1963.

63. Gianotta, S. F., Proceedings of the Eighth International Conference on Phenomena in Ionized Gases, Vienna, (Vienna: Springer-Verlag), p. 62, 1967.

64. Smith, C. G., "Motion of an 'Anchored' Arc Impelled by a Magnetic Field," Physical Review, v. 82, p. 570, 1951.

65. St. John, R. M., and Winans, J. G., "Motion and Spectrum of Arc Cathode Spot in a Magnetic Field," Physical Review, v. 98, p. 1664-1671, June 1955.

66. Kesaev, I. G., Cathode Processes of an Electric Arc, (in Russian), Nauka Press, Moscow, 1968.

67. Robson, A. E., and Von Engel, A., "Motion of a Short Arc in a Magnetic Field," Physical Review, v. 104, p. 15, 1956.

68. Poeffel, K., "Influence of the Copper Electrode Surface on Initial Arc Movement," IEEE Transactions on Plasma Science, v. PS-8, No. 4, p. 443-448, December 1980.

69. Rothstein, J., "Holes and Retrograde Arc Spot Motion in a Magnetic Field," _Physical Review_, v. 78, p. 331, 1950.

70. Longini, R. L., "A Note Concerning the Motion of Arc Cathode Spots in Magnetic Fields," _Physical Review_, v. 71, p. 642-643, 1947.

71. Guile, A. E., and Seeker, P. E., "Arc Cathode Movement in a Magnetic Field," _Journal of Applied Physics_, v. 29, p. 1662-1667, December 1958.

72. Hull, A. W., "Cathode Spot," _Physical Review_, v. 126, No. 5, p. 1603-1610, June 1962.

73. Sena, L. A., "Possible Mechanism for the Retrograde Motion of a Cathode Spot," _Soviet Physics: Technical Physics_, v. 13, No. 11, May 1969.

74. Robson, A. E., "The Motion of a Low Pressure Arc in a Strong Magnetic Field," _Journal of Physics D: Applied Physics_, v. 11, p. 1917-1923, 1978.

75. Auweter-Ming, M., and Schrade, H. O., "Exploration of Arc Spot Motion in the Presence of Magnetic Fields," _Journal of Nuclear Materials_, v. 93 & 94, p. 799-805, 1980.

76. Smith, C. G., "Motion of an Arc in a Magnetic Field," _Journal of Applied Physics_, v. 28, p. 1328-1331, November 1957.

77. Robson, A. E., _Proceedings of the Fourth International Conference on Ionization Phenomena in Gases_, Uppsala, (Amsterdam: North Holland), v. 1, p. 346, 1959.

INITIAL DISTRIBUTION LIST

		No. Copies
1.	Defense Technical Information Center Cameron Station Alexandria, Virginia 22314	2
2.	Library, Code 0142 Naval Postgraduate School Monterey, California 93940	2
3.	Department Chairman, Code 61 Department of Physics and Chemistry Naval Postgraduate School Monterey, California 93940	1
4.	Assoc. Professor F. R. Schwirzke, Code 61Sw Department of Physics and Chemistry Naval Postgraduate School Monterey, California 93940	3
5.	Professor K. E. Woehler, Code 61 Wh Department of Physics and Chemistry Naval Postgraduate School Monterey, California 93940	1
6.	LCDR Franklin T. Ryan, USN 21 Shubrick Road Monterey, California 93940	2
7.	CDR Stephen T. Shedd, USN USS Charles F. Adams (DDG-2) FPO New York, New York 09501	2